An Adaptive Ground Motion Prediction Equation for use in Low-to-moderate Seismicity Regions

Yuxiang Tang[a]*, Nelson Lam[a,c], Hing-Ho Tsang[b,c], Elisa Lumantarna[a,c]

[a]*Department of Infrastructure Engineering, University of Melbourne, Melbourne, Australia;*

[b]*Department of Civil and Construction Engineering, Swinburne University of Technology, Melbourne, Australia;*

[c]*Bushfire and Natural Hazards Cooperative Research Centre, Melbourne, Australia.*

The University of Melbourne, Parkville, VIC 3010, Australia. Email: yuxiang.tang@unimelb.edu.au

An Adaptive Ground Motion Prediction Equation for Use in Low-to-moderate Seismicity Regions

In regions of low-to-moderate seismicity where representative strong motion data is lacking, the modelling of seismic hazard relies on the use of seismological models. This paper presents a set of expressions that can be used as ground motion prediction equations that have been transformed from seismological models which resolve the generation of seismic waves into several components. The feature of this presented set of expressions is that it can be adapted to represent earthquake ground motion behaviour that is defined by a diversity of seismological models. The motivation behind the development of the presented adaptive predictive relationship which is known as the *Component Attenuation Model* (**CAM**) was to fast track, and make transparent, the transformation from seismological models to predictions of response spectral values for engineering applications. Thus, **CAM** can be used to waive away the need of executing any software for undertaking stochastic simulations nor time-history analyses for calculation of the response spectral ordinates. An important, and original, feature of **CAM** is incorporating the shear wave velocity profile of the bedrock and the associated upper-crustal modification into the model. This article presenting **CAM** is essentially an original contribution to engineering as opposed to seismology. The potential benefits derived from the fast-tracking can be considerable given that the transformation is seldom a one-off process and would need to be repeated for any given targeted area, in view of uncertainties surrounding seismological conditions of the earth crust around the globe.

Keywords: component attenuation model; ground motion prediction equations; attenuation parameter; upper-crustal modification

Introduction

The empirical modelling of Ground Motion Prediction Equation (GMPE) requires an abundant supply of strong motion data to cover for earthquake scenarios that are of engineering interests. This conventional approach to modelling is only viable in tectonically active areas that have been installed with an adequately dense strong motion instrumental recording network for many years. In stable regions of low-to-moderate seismicity (away from tectonic plate margins), stochastic simulation of the seismological model has been established for several decades in lieu of conventional empirical modelling. This alternative method of ground motion modelling is required to overcome challenges that are resulted from the lack of strong motion data.

In the seismological model, the *Fourier Amplitude Spectrum* (**FAS**) of earthquake ground motion is expressed as a product of numerous factors representing the effects of the source (incorporating magnitude scaling), geometrical attenuation, anelastic attenuation and crustal modification close to the earth surface (e.g. Atkinson and Boore [1995]; [1998]). A generic frequency dependent source scaling relationship for intraplate earthquakes that was initiated in a personal communication between Boore and Atkinson [1992], published in Atkinson [1993] and Atkinson and Boore [1995], updated in Atkinson and Silva [2000], and further developed in Boore *et al*. [2004] has been generalised to stable (intraplate) areas in general in order that only parameters characterising the path factors need to be found to complete the stochastic model for a diversity of environment. Attributed to the development of generic source factor in the seismological model only the path and site factors would need to be determined, and this is normally accomplished by calibration against empirical information derived from the seismological monitoring of small magnitude events. Consequently, there is not a need to curve-fit empirical strong motion data when developing a representative ground motion model for an intraplate region.

Once a representative seismological model for the study region has been developed strong motion accelerograms can be simulated by the computer and this involves assigning random phase angles to the individual sinusoids constituting the acceleration time-histories on the ground surface (as explained in a review article by Lam *et al*. [2000a]). Standard calculation procedures may then be applied to derive the response spectrum for any given earthquake scenario. A GMPE for the targeted intraplate area may then be developed by systematically repeating the simulation (and calculation) process for the whole range of **M - R** combinations.

To address the drawbacks of using stochastic simulations of a seismological model for predicting ground motion behaviour additional features of a seismological model have been incorporated in a series of updates over the years (the more recent updates being: Boore *et al*. [2014]; Yenier and Atkinson [2014]; Yenier and Atkinson [2015a]; Yenier and Atkinson [2015b]; Hassani and Atkinson [2018]). Many versions of seismological models have been developed for the well-studied region of Eastern North America (ENA) where there is an abundance of seismological information to constrain parameter values. Recommendations (of the most preferred six models) have been proposed in a *Pacific Centre of Earthquake Engineering* (PEER) publication forming part of the PEER NGA-East ground motion modelling project [Boore, 2015].

Notwithstanding, the complexities in the earthquake generation process and the quantification of the random uncertainties (that are embodied in a conventional empirical model) cannot possibly be fully captured by the seismological model nor by any associated stochastic modelling process. The adoption of the *Hybrid Empirical Method* (**HEM**) of modelling which was first introduced by Campbell [2003] was motivated by this intrinsic deficiency of a fully stochastic model. The GMPE of Pezeshk *et al*. [2015] for Eastern North America was developed using the **HEM** methodology. Another modelling approach which involves making adjustment to an existing empirical GMPE model is the *Referenced Empirical Method* (**REM**) which has been implemented in many areas as reported in Atkinson [2008], Atkinson and Boore [2011], Atkinson and Motazedian [2013] and Hassani and Atkinson [2015]. This method of modelling is only viable if there is adequate strong motion data in both the (relatively more stable) "targeted" region and the (much more active) "reference" region. A GMPE which was derived using the **REM** approach in Atkinson [2008] for Eastern North America reveals broad agreement with predictions from the fully stochastic model of Atkinson and Boore [2006]. In summary, both the (fully) stochastic modelling methodology and **HEM** remain to be viable means of deriving GMPEs for a region where representative strong motion data is at a paucity.

Although the stochastic simulation methodology has been well established for many years, deriving a definitive solution for the GMPE in a "data poor" region is not straightforward, and more so for areas that have not been well studied. From the engineering perspectives, it would be beneficial to have the stochastic process fast-tracked, and made transparent, to allow for the need to undertake multiple trials of stochastic simulations to trend the effects of changing input parameter values in order that the engineering significance of the modelling uncertainties can be observed readily. The widely used world acclaimed software **SMSIM** [Boore, 2003] that can be used for processing stochastic simulations is available for free internet download (http://www.daveboore.com). Program **GENQKE** that was written by the second author is also offered for free [Lam *et al*., 2000a]. A software has also been developed by the first author in the MATLAB environment to expedite its utility. Even then, a facility to

transform seismological parameters into GMPE parameters without the need of executing any computer software at all is by far more expedient.

The latest development of stochastic modelling as presented by Yenier and Atkinson [2015b] and Hassani and Atkinson [2018], which is abbreviated herein as **YA15** and **HA18**, is to have response spectral ordinates (along with peak ground acceleration and velocity) expressed in the form of algebraic expressions which comprise factors to represent the effects of various source, path and site modification mechanisms. The stochastic simulation process is therefore fast-tracked thereby waiving away the need to regularly execute software in undertaking the transformation from the *Fourier* domain to the time domain**.** The "plug-and-play" capability of these generic GMPEs provides coverage across different regions through the use of input parameters namely stress drop, geometrical spreading factor, anelastic attenuation function in addition to the usual parameters of magnitude, distance and site class which characterises the seismological characteristics of the target region. These models can be used to facilitate exploration of the response spectral sensitivity of earthquake ground motions to changes in the regional seismological conditions (amid epistemic uncertainties that have not been resolved). In essence, a seismological model expressed in the *Fourier* domain is transformed into a GMPE in a transparent manner allowing users to make adjustments to the input information to suit a diversity of local (regional) site conditions.

The Component Attenuation Model

The GMPE to be introduced in this article which is referred herein as the Component Attenuation Model (**CAM**) is a regionally adjustable GMPE following the format of **YA15** and **HA18** for transforming seismological models into GMPEs and is specifically targeted for use in stable areas of low-to-moderate seismicity. **CAM** features the use of a geology-based crustal modelling approach wherein crustal shear wave velocity profiles of bedrock to depths of tens of kilometers were employed to derive upper-crustal amplification factors forming part of **CAM** (not to be confused with site amplification factors for modelling modification mechanisms of the surface soil sediments typically down to depths of tens of meters only). The crustal structure of bedrock is a very important element of considerations in ground motion modelling [Burger *et al*., 1987; Chandler *et al*., 2006a; Chandler *et al*., 2006b]. However, existing GMPEs that are used nowadays are simply based on general broad geographical sub-division of a region like the Middle East [Ambraseys *et al*., 2005], Eastern North America [Atkinson and Boore, 1995; Atkinson, 2004; Atkinson and Boore, 2006; Atkinson, 2008; Atkinson and Boore, 2014; Yenier and Atkinson, 2015b], Western Australia [Allen *et al*., 2006; Liang *et al*., 2008], South Eastern Australia [Allen, 2012]. In situations where the geological structure varies significantly within a region (e.g. Eastern China as reported in Tsang *et al*. [2010]) no one existing GMPE is able to represent the intra-regional variability. **CAM** is proposed herein as the modelling methodology to take into account variability in the crustal structure for resolving uncertainties.

In **CAM** an upper-crustal modification factor ($\boldsymbol{\gamma_{uc}}$) is introduced alongside the geometrical and anelastic attenuation factors (**G** and $\boldsymbol{\beta}$) to provide coverage for the filtering behaviour of the upper crust. Surveying the shear wave velocity profile of the upper crust (bedrock down to depth of 10 km) involved monitoring micro-tremors (background noise) using an array of geophones and monitoring blast generated ground shocks in combination with seismological surveys as described in Chandler *et al*. [2006a]. The upper-crustal amplification factor which is frequency dependent is then derived from the surveyed crustal shear wave velocity profile. This method of modelling the filtering characteristics of the earth crust put less reliance on locally recorded ground motions.

As pointed out in Boore *et al*. [2010] and Yenier and Atkinson [2014], placing full reliance on stochastic simulations to match recorded spectrum for determining input parameters into the generic GMPE may produce non-unique solutions and compromise accuracy because of trade-offs between the source and path components of the GMPE. This trade-off issue (intrinsic drawback of stochastic simulation based GMPEs) can be circumvented by making use of information separate to the recorded ground motion data to constrain input information. In an intraplate environment where locally recorded ground motion records are too sporadic to constrain an input parameter into the GMPE, isolated ground motion data can be used instead to spot check modelling errors provided that input information into the model has been obtained from alternative sources.

The original form of **CAM** which first presented in Lam *et al*. [2000b] was very restrictive as only three ground motion parameters can be predicted. This article presents the updated version of **CAM** which provides estimates for response spectral ordinates as for most contemporary GMPEs. In this section, the functional form associated with each of the component factors in **CAM** is introduced, under separate sub-headings. In the next Section **CAM** is verified by (i) applying it to transform six well known seismological models from the (original) *Fourier amplitude spectrum* format into the respective GMPEs in the time domain, and (ii) making direct comparisons of predictions by **CAM** with that obtained from use of the generic GMPEs of **YA15** and **HA18**. Further validations are then undertaken by comparison of response spectral parameters recorded from 12 earthquake events recorded in Switzerland (of magnitude varying from **M**4 to **M**5） with predictions by **CAM**.

The framework of **CAM** as an adaptable GMPE is of a multiplicative format similar to the seismological model which decouples the source and attenuation effects into different components as shown by Eq. (1)

$$\mathbf{Y} = \Delta \times \boldsymbol{\alpha} \times \boldsymbol{\beta} \times \mathbf{G} \times \boldsymbol{\gamma_{uc}} \times \mathbf{C} \tag{1}$$

The transmission of seismic waves through softer surficial sedimentary layers (or hydraulic fills) are not covered by **CAM** in view of contemporary engineering design practice of employing soil dynamic analyses (using information inferred from borelogs on a site-by-site basis as input) for undertaking this component of ground motion modelling. The effects of

multiple reflections in between boundaries of individual soil layers can be modelled by this form of analysis.

CAM can also be presented in the logarithmic (base 10) format as shown by Eq. (2):

$$\log\mathbf{Y} = \log\Delta + \log\boldsymbol{\alpha} + \log\boldsymbol{\beta} + \log\mathbf{G} + \log\boldsymbol{\gamma_{uc}} + \log\mathbf{C} \quad (2)$$

where, **Y** is the (orientation-independent) predicted ground motion intensity measure (response spectral acceleration in this study) assuming 5% damping, Δ is the referenced intensity measure for a referenced scenario (e.g. **M** = 6, **R** = 30), **α** is the source factor, which is function of the earthquake moment magnitude (**M**) and Brune stress drop **(**$\Delta\boldsymbol{\sigma}$), **β** is the path factor which is responsible for the attenuation effects excluding geometric attenuation (**G**), **G** is the geometric attenuation factor shaping *Fourier Amplitude Spectrum* (FAS), $\boldsymbol{\gamma_{uc}}$ is the upper-crustal modification factor which accounts for upper-crustal amplification and attenuation phenomena within the rock crust, and **C** is the calibration factor (which is to minimise discrepancies between the model predictions and empirical recordings). An overview of the modelling parameters introduced above is summarised in Table 1.

Values of the reference intensity (Δ in Eqs. (1) and (2)) which is based on response spectral estimates for the reference condition of **M** = 6, **R** = 30 on rock sites as listed in Table 2 are based on the (usual) geometrical attenuation model of **G** = 1/**R**. Should a different **G** model is adopted (e.g. **G** = $\mathbf{R}^{-1.3}$) the listed reference values would require adjustments or else **CAM** could give over-predictions at distance closer than 30 km. In any case, the listed reference values can be supplanted by the user should relevant and reliable information become available to constrain the ground motion intensity at **M** =6 and **R** = 30 km.

Table 1. Parameter values used in stochastic simulations.

Parameter	Value
Source shear-wave velocity	3.8 km/s by default
Source density	2.8 g/cm^3 by default
Source model	Generalized additive double-corner frequency model [Boore *et al*., 2014]
Spectral sag	$10^{0.605-0.255\mathbf{M}}$ [Yenier and Atkinson, 2014]
Distance	Hypocentral distance
Geometrical attenuation model	Variable functions refer to Table A1 in the Appendix
Anelastic attenuation model	$Q = Q_0 f^n$, Q_0=120, 150, 200, 300, 400, 500, 600, 680, 800. $n = 0.0000008Q_0^2 - 0.0014Q_0 + 0.93$ [Mak *et al*., 2004]
Upper-crustal amplification	V_{S30}=0.618, 0.76, 1.0, 1.2, 1.4, 1.6, 1.8, 2.0, 2.2, 2.4, 2.6, 2.78 km/s
Upper-crustal attenuation	κ_0= 0.001, 0.0025, 0.005, 0.0075, 0.01, 0.015, 0.02, 0.025, 0.03, 0.035, 0.04, 0.045, 0.05, 0.055, 0.06, 0.065, 0.07, 0.075, 0.08, 0.085, 0.09, 0.095, 0.1 s
Source duration	$0.5/f_a + 0.5/f_b$, where f_a and f_b are the corner frequencies
Path duration	0.05 × **R**, where **R** is the hypocentral distance

Source factor

The source factor is of the form shown by Eq. (3).

$$\log\boldsymbol{\alpha} = a_1 \times \mathbf{M}^{a_2} \times \Delta\boldsymbol{\sigma}^{a_3} + a_4 \quad (3)$$

where, a_1 - a_4 are period-dependent model coefficients, **M** is the moment magnitude and $\Delta\boldsymbol{\sigma}$ is the Brune stress drop in bar. Eq. (3) was derived from the simulated data which have been normalised at **M** = 6. The model covers the range: **M**4 - **M**8 and $\Delta\boldsymbol{\sigma}$ = 30 - 300 bars.

The underlying seismological model for source effects is of the generalised form of the double-corner frequency model (of the "additive" option) as proposed by Boore *et al*. [2014]. The *Fourier Amplitude Spectrum* representing the source model is defined by the following series of equations.

$$A_0(f) = (2\pi f)^2 C\mathbf{M}_0\left[\frac{1-\varepsilon}{1+(f/f_a)^2} + \frac{\varepsilon}{1+(f/f_b)^2}\right] \quad (4)$$

in which,

$$log f_a = 2.181 - 0.496\mathbf{M} \quad (5a)$$

$$log\varepsilon = 0.605 - 0.255\mathbf{M} \quad (5b)$$

$$f_0 = 4.906 \times 10^6 \beta_0 (\Delta\boldsymbol{\sigma}/\mathbf{M}_0)^{1/3} \quad (6)$$

$$f_b = \left[\frac{f_0^2 - (1-\varepsilon)f_a^2}{\varepsilon}\right]^{1/2} \quad (7)$$

$$C = (R_\emptyset VF)/(4\pi\rho_{sim}\beta_{0sim}^3) \quad (8)$$

In the equations shown above, f_0 , f_a , f_b are the corner frequencies (Hz), $R_\emptyset$ is the *radiation parameter* (equals to 0.55 on average for shear waves), *V* is the partitioning of seismic energy onto horizontal component (0.71), *F* is the *free surface amplification factor* (2.0), $\mathbf{M}_0$ is the *seismic moment*, where $\mathbf{M}_0 = 10^{1.5(\mathbf{M}+10.7)}$. ρ_{sim} (2.8 g/cm^3 be default) and β_{0sim} (3.8 km/s be default) represent the density and shear wave velocity respectively at the depth of the source that have been adopted in the stochastic simulations.

Another source parameter that is relevant to simulating ground motions is the duration of the strong motion. The following expression for estimating the duration of motion is based on resolving the total duration as a sum of the source duration and path duration as shown by Eq. (9a).

$$T = T_0 + d\mathbf{R} \quad (9a)$$

where *d* = 0.05 is taken for all conditions. Equal weights have been assigned to the two corner frequencies in deriving the source duration as shown by Eq. (9b).

$$T_0 = 0.5\frac{1}{f_a} + 0.5\frac{1}{f_b} \quad (9b)$$

Results generated from the stochastic simulation of the seismological model are shown in Fig. 1 alongside predictions of the source factor $\boldsymbol{\alpha}$ (forming part of **CAM**).

Predictions by Eq. (3) for value of $\boldsymbol{\alpha}$ which provides response spectral acceleration (RSA) values that have been normalised with respect to **M** = 6 and **R** = 30 km, and based on $\Delta\boldsymbol{\sigma}$ = 200 bars (which is considered to be a reasonable assumption to make for intraplate conditions) are presented in Fig. 2(a)**.** RSA values that have been normalised with respect to $\Delta\boldsymbol{\sigma}$ = 200 bars and **R** = 30 km (for **M** = 6) are presented in Fig. 2(b) to show the influence of the stress parameter. The value of RSA is shown to become more sensitive to changes in the value of **M** with increasing natural period, but less sensitive to changes in the value of stress drop with increasing natural period.

The next step of the model development is to make use of existing seismological information to determine values of **β** (the path factor) to take into account regional attenuation behaviour of the earth crust (separate to the upper-crustal modification effects which are addressed in the following section).

Path factor

The path factor (**β**) is to account for the attenuation effects of the ground motions along the entire transmission path of the seismic wave from the source to the site. In **CAM**, as for most seismological models, the attenuation behaviour that is associated with the spatial spread of energy is taken into account by another factor: Geometric attenuation factor (**G**). Thus, the **β** factor is only to model the part of the attenuation that is associated with the dissipation of energy by the inelastic behaviour of the crustal medium. In deriving the value of **β**, results from stochastic simulations of the seismological models with increasing distance were normalised at **R** = 30 km and having the effects of geometric attenuation removed (as was to be accounted for by a separate factor).

The **β** factor so derived is expressed in form of Eq. (10):

$$\log\boldsymbol{\beta} = (b_1 * \mathbf{M} + b_2) \times \left(Q_0^{b_3}\right) \times ((\log\mathbf{R})^{b_4}) + b_5 \qquad (10)$$

where, b_1 - b_5 are the period-dependent model coefficients, **M** is the moment magnitude, Q_0 is the regional dependent quality factor for wave transmission and **R** is the hypocentral distance.

In Fig. 3 results from regression analysis of the stochastic simulated data that were used to define the modelled value of **β** (Eq. (10)) are shown for a range of Q_0 values (for **M** = 6). The stochastically simulated values are shown to match values predicted by Eq. (10) with good consistencies except for the minor discrepancies at T_n = 5.0 s. The stochastically simulated values of RSA are shown in Fig. 4 alongside predictions by **CAM** based on combining various factors representing contributions by the "source" and the "path" to the transmitted shear waves as per Eqs. (1, 3 and 8) taking **M** = 6, **G** = 1/**R**, Q_0 = 680, and $\boldsymbol{\gamma_{uc}}$ = 1.0. This dataset of simulated results and predictive calculations by **CAM** were then subject to residual

analysis wherein the residual value is defined as $\delta = \log(\mathbf{Y}_{sim}/\mathbf{Y}_{pred})$, where $\mathbf{Y}_{sim}$ and $\mathbf{Y}_{pred}$ are intensity measurements obtained from simulations and model predictions respectively. $\delta > 0$ refers to underestimation of **CAM** and $\delta < 0$ means overestimation of **CAM**. A 4th order polynomial expression (Eq. (11)) for defining the value of the adjustment factor $\boldsymbol{\beta}_{adjustment\_factor}$ is used to adjust, through multiplication, predicted values of $\boldsymbol{\beta}$ from Eq. (10) to minimise the values of the residuals and any systematic modelling errors.

$$\boldsymbol{\beta}_{adjustment\_factor} = b_6\mathbf{R}^4 + b_7\mathbf{R}^3 + b_8\mathbf{R}^2 + b_9\mathbf{R} + b_{10} \quad (11)$$

where, values of coefficients b_6 to b_{10} are listed in Table 2.

Values of the overall residuals (following application of the adjustment factor) are shown in Fig. 5, which demonstrates that the (curve-fitted) predictive model presented herein can make reasonably accurate predictions of the ground motion intensity measures for all distances, and for the magnitude range of **M**4.5 – **M**7.5. Individual values of the residuals are mostly within 0.1 unit. The value of the mean residual is close to zero, and with no apparent trending of the residual values with distance.

It is noted that the geometrical factor (**G**) provisions in most seismological models have not taken into considerations near distance saturation which can be accounted for by the introduction of the pseudo-depth term ([Yenier and Atkinson, 2015b] which is abbreviated herein as **YA15**). The ground motion intensity can be overestimated at near distances if this phenomenon has been neglected.

In a low-to-moderate seismicity region the hazard factor (i.e. the design peak ground acceleration) is typically not higher than 0.12g (or peak ground velocity of the order of 100 mm/s). **M** - **R** combinations which match with this ground motion intensity (based on median predictions) in places like southeastern Australia are expected to be **M**5.5 **R** = 15 - 20 km or **M**6 **R** = 25 - 30 km. For example, the iso-seismal map of the 1989 (**M**5.6) Newcastle earthquake which occurred at New South Wales, Australia shows **MMI** = VII in areas of rock outcrops at epicentral distances ranging between 15 and 20 km. With those earthquake scenarios introducing the pseudo-depth term (refer **YA15**) to allow for saturation effects would not result in more than 10% difference in the value of **R**. The effects of distance-saturation which is significant only in near source location of large magnitude earthquakes have accordingly not been modelled for reason of simplicity (i.e. $\mathbf{R} = \mathbf{R}_{rup}$, $\mathbf{R}_{rup}$ is the rupture distance). The use of a magnitude dependent term in the calculation of the Geometrical factor to allow for differences in the rate of attenuation in the Fourier and response spectral domains have also been omitted noting that errors arising from neglecting the difference is minor (when not applying corrections to allow for distance-saturation). Although the size of errors resulted from neglecting near distance saturation is expected to be minor in the context of modelling for regions of low-to-moderate seismicity it is important for users of GMPE's derived from seismological models (such as **CAM**) to be aware of this type of errors and their

extent. Notwithstanding, the construct of **CAM** provides the flexibility to have the near-distance saturation phenomenon to be taken into account.

Local upper-crustal modification factor

The *local upper-crustal* modification factor $\boldsymbol{\gamma_{uc}}$ is to account for the combined effects of amplification and attenuation of the upper earth crust which is mainly dependent on the shear wave velocity profile in the upper earth crust [Boore and Joyner, 1997]. Those phenomena are referred in the literature as upper crustal modifications. The modification factor can be resolved into three components: (i) amplification of the upper-crust; (ii) attenuation of the upper-crust; and (iii) modification of the mid-crust. The respective factors representing each of these components are combined in a multiplicative manner as represented by Eq. (12).

$$\boldsymbol{\gamma_{uc}} = \boldsymbol{\gamma_{am}} \times \boldsymbol{\gamma_{an}} \times \boldsymbol{\gamma_{mc}} \tag{12}$$

where $\boldsymbol{\gamma_{am}}$, $\boldsymbol{\gamma_{an}}$, and $\boldsymbol{\gamma_{mc}}$ are factors representing amplifications of upper crust, attenuation of the upper crust and modification of the mid-crust, respectively. Details of derivation of each of these component factors contributing to crustal modifications are described in the rest of this section under separate sub-headings.

Upper-crustal amplification ($\boldsymbol{\gamma_{am}}$)

In modelling upper-crustal amplification in this study, information presented in Boore and Joyner [1997] which is abbreviated herein as **BJ97,** and more recent updates [Boore, 2016] of the model have been adopted to construct shear-wave velocity profiles along with the inferred density profiles reported in Brocher [2005] to derive the upper-crustal amplification factors based on the use of the *square-root-impedance* (SRI) method. The shear-wave velocity profiles adopted in this study have been constructed using the slowness interpolation method [Boore, 2016]. Twelve shear wave velocity profiles that are characterised by parameter V_{S30} (time-averaged shear wave velocity in the upper 30 meters of the earth crusts) ranging from 0.618 km/s (generic rock) to 2.78 km/s (generic very hard rock) have been incorporated into the parametric study to derive values of the upper-crustal amplification factor. The modelled shear-wave velocity profiles and the corresponding frequency-dependent amplification factors so obtained from the analysis as described are presented in Fig. 6 and Fig. 7, respectively.

The upper-crustal amplification factor $\boldsymbol{\gamma_{am}}$ was derived accordingly as a function of V_{S30} by curve-fitting simulated data. The general form of the function is shown by Eq. (13).

$$\log\boldsymbol{\gamma_{am}} = \gamma_1 * V_{S30}^{\gamma_2} + \gamma_3 \tag{13}$$

where, γ_1 to γ_3 are period dependent coefficients. The predicted values are shown alongside results from numerical simulated values in Fig. 8.

No noticeable correlation between moment magnitude (**M**) and $\boldsymbol{\gamma_{am}}$ can be identified. Thus, $\boldsymbol{\gamma_{am}}$ is expressed as sole function of V_{S30}.

Upper-crustal attenuation ($\boldsymbol{\gamma_{an}}$)

In modelling upper-crustal attenuation which affects high frequency properties of the transmitted shear waves, the *Kappa* parameter (κ_0) was used as the key controlling parameter. Numerous studies that were targeted at modelling the value of κ_0 have been reported in the literature [Silva *et al*., 1999; Chandler *et al*., 2006; Drouet *et al*., 2010; Edwards *et al*., 2011; Van *et al*., 2011]. The maximum value of κ_0 that has been reported in the literature is 0.19 s for NEHRP site class E [Silva *et al*., 1999]. In this study, maximum κ_0 value of 0.1s is taken for rock sites. In the simulations undertaken in this study, the value of κ_0 accordingly ranges from 0.001s to 0.1 s. The functional form of the expression for determining the values of $\boldsymbol{\gamma_{an}}$ to incorporate the effects of upper-crustal attenuation is represented by Eq. (14).

$$\log\boldsymbol{\gamma_{an}} = \gamma_4 * \mathbf{M}^{\gamma_5}\kappa_0^{\gamma_6}+\gamma_7*\kappa_0 +\gamma_8 \tag{14}$$

where, γ_4 to γ_8 are period dependent coefficients

Results shown in Fig. 9 are consistent with observations by Yenier and Atkinson [2015b] that the value of κ_0 affects the response spectrum more at short periods than that at long periods. When the value of κ_0 is less than 0.01 s the effects of upper-crustal attenuation on the response spectral amplitude at 0.3 s period can be ignored; the limiting value of κ_0 is relaxed to 0.1 s when predicting response spectral amplitude at 1.0 s period.

Mid-crustal modification ($\boldsymbol{\gamma_{mc}}$)

Another crustal factor is called the mid-crustal modification factor $\boldsymbol{\gamma_{mc}}$, which is to account for the effects of the density and shear-wave velocity of the earth crust at the depth of the source of the earthquake, and its value can be found using Eq. (15).

$$\boldsymbol{\gamma_{mc}} = \frac{\rho_{sim}\beta_{0sim}^{n}}{\rho_S\beta_{0S}^{n}} \tag{15}$$

where, ρ_{sim} and β_{0sim} are the density and shear-wave velocity respectively used in the stochastic simulations undertaken in this study: ρ_{sim} = 2.8 g/cm^3 and β_{0sim} = 3.8 km/s, whereas ρ_S and β_{0S} are the actual density and shear-wave velocity at the depth of the source. The value of the exponent *n* is changed with different conditions. Take *n* = 1 for the

prediction of response spectral acceleration, n = 2 for velocity and n = 3 for displacement. Values of all the regression coefficients constituting **CAM** are summarised in Table 2.

Verification of CAM

An important objective of this article is having **CAM** verified and demonstrating its utility in transforming seismological models (presented in the form of a *Fourier Amplitude Spectrum*) into GMPEs. In Part One of this section which is aimed at verifying **CAM** six well known seismological models that have been developed for use in ENA (refer Table A1 in the Appendix) have been translated into GMPEs. The considered seismological models which have been shortlisted in the review article by Boore [2015] are namely: Atkinson and Boore [1995] referred as **AB95**, Silva *et al*. [2002] referred as **SGD02**, Atkinson [2004] referred as **A04**, Boore *et al*. [2010] referred as **BCA10d,** Boatwright and Seekings [2011] referred as **BS11** and Atkinson and Boore [2014] referred as **AB14.**

Table 2. Model Coefficients for **CAM.**

Tn (s)	Δ	logα				logβ										logγ							
		a_1	a_2	a_3	a_4	b_1	b_2	b_3	b_4	b_5	b_6	b_7	b_8	b_9	b_{10}	γ_1	γ_2	γ_3	γ_4	γ_5	γ_6	γ_7	γ_8
0.01	0.9859	0.658	0.5136	0.185	-4.416	0.0306	-0.512	-0.214	3.286	0.3401	0.2288	-1.253	2.192	-1.559	0.4035	-19.15	0.0227	19.68	-7.361	-0.156	0.1813	0.6193	1.432
0.02	0.7350	0.638	0.5235	0.187	-4.399	0.0206	-0.329	-0.243	3.824	0.2256	0.2989	-1.861	3.946	-3.451	1.045	2.876	-0.135	-2.414	-10.24	-0.209	0.3884	4.425	0.4725
0.03	0.6242	0.728	0.5093	0.175	-4.575	0.0160	-0.253	-0.267	4.183	0.1828	0.2599	-1.661	3.643	-3.302	1.02	1.679	-0.225	-1.253	-16.02	-0.186	0.5656	10.2	0.2491
0.05	0.4702	0.833	0.4958	0.164	-4.804	0.0119	-0.185	-0.304	4.629	0.1324	0.1421	-0.923	2.068	-1.941	0.6394	1.221	-0.294	-0.812	-83.48	-0.045	0.9081	77.79	0.0944
0.10	0.3052	2.709	0.3409	0.073	-7.343	0.0094	-0.150	-0.389	5.13	0.0924	0.0101	-0.061	0.1328	-0.176	0.1003	0.764	-0.426	-0.402	9.581	0.3886	1.65	-15.99	0.0137
0.14	0.2436	4.834	0.2648	0.045	-9.833	0.0945	-0.149	-0.437	5.296	0.0712	-0.010	0.0880	-0.233	0.1876	-0.026	0.489	-0.636	-0.164	3.372	0.6984	1.943	-10.41	0.0053
0.18	0.1949	6.901	0.2218	0.032	-12.16	0.0115	-0.180	-0.490	5.337	0.0647	-0.006	0.0615	-0.171	0.1366	-0.016	0.5184	-0.576	-0.198	-169	-0.005	0.9927	162.7	0.0184
0.22	0.1615	10.57	0.1742	0.021	-16.11	0.0119	-0.194	-0.526	5.369	0.0566	-0.007	0.0645	-0.184	0.1569	-0.038	0.4157	-0.686	-0.117	-291.4	-0.000	0.9974	285.7	0.0104
0.30	0.1169	6.999	0.2399	0.028	-12.44	0.0149	-0.227	-0.578	5.419	0.0424	-0.007	0.0591	-0.167	0.1427	-0.016	0.3446	-0.813	-0.073	-2.992	-0.493	0.7827	-2.713	0.0055
0.40	0.08625	23.00	0.11	0.008	-29.25	0.0195	-0.276	-0.628	5.476	0.0447	0.0048	-0.005	-0.046	0.0656	-0.066	0.3081	-0.776	-0.087	-8.008	-2.094	0.4837	-3.108	0.0139
0.50	0.06089	20.54	0.1262	0.008	-26.94	0.0202	-0.283	-0.661	5.556	0.0349	-0.003	0.0536	-0.199	0.222	-0.089	0.2685	-0.871	-0.051	-17.21	-2.645	0.4594	-2.603	0.0083
0.60	0.04494	57.92	0.0550 3	0.003	-64.92	0.0234	-0.320	-0.699	5.585	0.0317	0.0044	-0.002	-0.051	0.0586	-0.022	0.2036	-1.070	0.0027	-30.09	-2.984	0.46	-2.216	0.0074
0.70	0.03377	24.00	0.118	0.006	-30.62	0.0283	-0.376	-0.741	5.639	0.0261	0.0045	-0.001	-0.060	0.0814	-0.009	0.1646	-1.254	0.0349	-30.09	-2.984	0.46	-2.216	0.0074
0.80	0.0278	10.67	0.2202	0.011	-16.9	0.0307	-0.391	-0.759	5.696	0.0223	0.0116	-0.048	0.0463	-0.021	0.0115	0.1434	-1.366	0.0264	-393.8	-4.77	0.4709	-1.825	0.0025
0.90	0.0232	24.53	0.1214	0.005	-31.4	0.0305	-0.389	-0.774	5.741	0.0184	0.0119	-0.051	0.0542	-0.032	0.0042	0.1474	-1.303	0.0067	-349.4	-4.629	0.4895	-1.636	-0.002
1.00	0.01949	25.97	0.1187	0.004	-32.96	0.0288	-0.363	-0.783	5.829	0.0092	0.0152	-0.076	0.1286	-0.123	0.0512	0.1215	-1.516	0.0204	-115	-3.738	0.4838	-1.415	0.0061
1.50	0.009236	21.50	0.1436	0.003	-28.46	0.0412	-0.473	-0.873	6.073	0.000	0.0210	-0.108	0.1937	-0.190	0.1101	0.1703	-0.806	-0.026	-483.5	-4.57	0.5104	-1.038	0.0017
2.00	0.005262	19.12	0.1598	0.003	-26.04	0.0772	-0.793	-0.990	6.301	-0.008	0.0151	-0.076	0.1392	-0.164	0.1386	0.1276	-1.14	0.0205	-254.1	-3.952	0.53	-0.741	0.0088
3.00	0.002435	26.56	0.1303	0.002	-34.08	0.1891	-1.713	-1.196	6.859	0.0046	0.0033	0.0069	-0.050	-0.022	0.1028	0.1062	-1.356	0.0230	-484.2	-4.315	0.5722	-0.585	0.0031
4.00	0.00134	23.95	0.1432	0.002	-31.36	0.4871	-4.202	-1.402	7.273	0.0141	-0.004	0.0697	-0.200	0.0916	0.1029	0.1039	-1.325	0.0167	-1144	-4.897	0.577	-0.596	-0.000
5.00	0.000825	9.008	0.2892	0.005	-15.58	2.271	-18.47	-1.597	7.171	0.0225	-0.014	0.1482	-0.418	0.308	0.0369	0.109	-1.223	0.0119	-2116	-5.348	0.609	-0.639	-0.011
6.00	0.000566	4.351	0.4345	0.010	-10.08	2.423	-19.30	-1.504	6.695	0.0235	-0.024	0.2388	-0.692	0.5819	-0.025	0.1084	-1.245	0.0138	-34470	-7.403	0.6309	-0.811	-0.019
8.00	0.000281	2.061	0.5977	0.025	-6.954	0.8278	-6.660	-1.226	6.161	0.0212	-0.024	0.2708	-0.805	0.6959	-0.044	0.1089	-1.336	0.0174	-60650	-7.77	0.6697	-1.007	-0.024

These seismological models contain different geometric attenuation and anelastic attenuation functions whereas the same source model has been specified (i.e. the generalised additive double-corner frequency model with stress drop of 200 bars). The value of the density and shear-wave velocity of the earth crust at the depth of the source are consistent amongst these models. Identical NEHRP B/C site conditions, with V_{S30} =0.76 km/s and κ_0 = 0.025 s as proposed by Yenier and Atkinson [2015b] have been adopted. The geometric attenuation factor as stipulated by the individual seismological model (refer to Table A1) is diverse. The following is a list of remarks highlighting certain distinctive features of the path components in each of the considered seismological models.

With **AB95** the exponent factor "*n*" in the Q factor ($Q = Q_0 f^n$) is fixed at 0.36 whereas $n = 0.0000008Q_0^2 - 0.0014Q_0 + 0.93$ has been adopted in **CAM** following the recommendations by Mak *et al*. [2004]. The geometric attenuation factor is of the tri-linear form. The density (2.8 g/cm^3) and shear-wave velocity (3.8 km/s) at the depth of the source are consistent with values used in **CAM** (as listed in Table 1). With **SGD02** the geometric attenuation factor is magnitude and distance dependent. With **BS11** the geometric attenuation is of the bi-linear form, and the Q_0 value (410) is relatively low. With **A04** the functional form of the Q factor is not of the typical form involving parameters Q_0 and *n* but is instead defined as follows: $Q(f) = \max(1000, 893f^{0.32})$. The value of Q_0 was set at 893 for $T_n < 1$ s, and at 1000 for $T_n \geq 1$ s. With **BCA10d** (as for **A04**) the Q factor is not of the typical form involving parameters Q_0 and *n*, but is instead fixed at value of 2850. Given this constraint, the equation $Q_0 f^n = 2850$ (in which, $n = 0.0000008Q_0^2 - 0.0014Q_0 + 0.93$) must be solved to find the exact value of Q_0 for a range of natural periods. The solution is: Q_0 = 1436 at T_n = 0.3 s, Q_0 = 1645 at T_n = 0.5 s, and for all periods exceeding $T_n \geq 1$ s, Q_0 = 2850. The "distance" term in the geometric attenuation model has incorporated finite-fault effects (based on the use of the h_{FF} factor). With **AB14** the geometric attenuation form is the effective point-source distance which has incorporated near-source saturation effects. A listing of the parameter values for each of the seismological model can be found in Table A1.

Comparisons are made between the stochastically simulated values of the 5% damped response spectral acceleration at designated natural periods of 0.3 s, 0.5 s, 1.0 s, and 5.0 s with values calculated using the algebraic expressions of **CAM**. The comparison as presented in Figs. 10(a) - 10(f) (for T_n = 0.3 s) shows good match for across all the considered seismological models and for all magnitude-distance combinations that are within the range of the comparison. Thus, the generic GMPE of **CAM** has been demonstrated to be able to accurately transform a diversity of seismological models into respective GMPEs. Similar consistencies have also been found for other natural periods which are not presented herein.

In Part Two of this section, direct comparisons between the generic (regionally adjustable) GMPEs of **CAM** and **YA15** (and **HA18**) are presented for varying magnitudes (Fig. 11), varying stress drop (Fig. 12), varying distance (Fig. 13), and varying κ_0 values incorporating

findings of Hassani and Atkinson (2018) which is abbreviated herein as **HA18** (Fig. 14). The comparisons are purely to demonstrate consistencies in their respective scaling relationships (no crustal factor nor site factor has been applied).

A "total" comparison between the two generic GMPEs (**CAM** and **YA15**) incorporating all component factors are shown in Fig. 15a and Fig. 15b for ENA and Californian (WNA) conditions respectively. It is shown in these figures that there are overall good consistencies between the two models apart from some noticeable conservatism of predictions by **CAM** in comparison with predictions by **YA15**. Ground motions in ENA are known to feature a higher stress drop and lower kappa values (which only affects the response spectrum in the short period range) and a lower rate of anelastic attenuation (which only affects ground motions at long distances). In addition to these well recognised differences there are other major (broad-band) differences in the ground motion behaviour between the two regions as reflected in the difference between the Calibration factors in the **YA15** model: C_{WNA} and (C_{eCENA}, C_{pCENA}), which is 0 and (-0.25, -0.15) respectively for natural period of 0.3 s. This difference in the calibration factor between the two regions is translated to a WNA/ENA response spectral ratio of 1.5 (being exp(0)/exp(-0.4)). This major regional difference is equally well reflected in results calculated from **CAM** (which is without a calibration factor) by virtue of its upper crustal factor. Thus, systematic differences between ground motions predicted for ENA and WNA for a given **M**-**R** combination are well reflected in **CAM** as much as in **YA15**.

Values of parameters adopted in **YA15** (**HA18**) and in **CAM** in the comparative analysis are listed in Table 3 and in the title of respective figures. The anelastic attenuation factor in **YA15** was derived from empirical analysis of ENA records. When using **CAM**, a Q_0 value of 680 which is considered to be representative of ENA conditions has been adopted. The site amplification factor adopted in **YA15** was inferred from empirical recordings on soil sites [Seyhan and Stewart, 2014]. However, this study is scoped to rock conditions only; thus, soil site effects are not considered.

In summary, **CAM** (as a generic GMPE) has been demonstrated to be able to represent the seismological models with a good level of accuracies in terms of providing predictions for the response spectral values at designated natural periods of 0.3 s, 0.5 s, 1.0 s, and 5.0 s for magnitudes of the range **M**4.5 – **M**7.5 and distance of 4 km to 800 km (except for **M**-**R** combinations where the level of ground shaking has little engineering significance or where the site is too close to the source of a very large magnitude earthquake). Consistencies between **CAM**, **YA15** and **HA18** have also been demonstrated.

Table 3. Input parameters of **YA15** (**HA18**) and **CAM** for comparison in Figs. 11 - 14.

Parameter	Input value
Moment magnitude (**M**)	4.0 - 8.0 (**M** = 6 for comparing other parameters)
Rupture Distance (km)	4 – 800 (**R** = 30km for comparing other parameters)
Reference RSA (Δ) (g)	0.2053 (T_n = 0.3 s);
(**CAM** only)	0.0499 (T_n = 1.0 s)
Stress drop (bar)	30 - 300 ($\Delta\boldsymbol{\sigma}$ = 200 bar for comparing other parameters)
Pseudo-depth (km)	$10^{-0.405+0.235*\mathbf{M}}$
G	$\mathbf{R}^{-1.3}$ for **R** <= 50 km $\mathbf{R}^{-0.5}$ for **R** > 50 km
Q_0 (**CAM** only)	680
κ_0	0.001 – 0.1 s

Comparison with field recorded ground motion data

Following from the verification analysis presented in the previous section, further comparison between predictions by **CAM** and field recordings are presented in this section. It is important to compare the predicted ground motions with real observations to demonstrate the viability of **CAM**. Given that the **CAM** framework is for transforming seismological models into response spectral attenuation models, regional specific parameters would be required for input into **CAM**. In this comparative exercise, the authors chose to compare data recorded in the earthquake-affected area with model predictions based on input parameters that had been derived from research in the same regions. The recorded horizontal strong motion 5% damped response spectral data from Switzerland has been compiled from the Swiss Seismological Service (SSS) database (http://seismo.ethz.ch/en/home/, which was last accessed by the authors in January 2019). Switzerland lies in European Alpine collision zone, and the region is typically characterised as low-to-moderate seismicity. The detailed information of the selected earthquake events is listed in Table 4.

Table 4. Selected Earthquake events in Switzerland.

No.	Origin Time (dd/mm/yyyy, UTC)	Lat [°]	Lon [°]	Depth [km]	Mw	Count of records
1	01/07/2017	46.49 N	7.10 E	4	4.0 (4.3 $\mathbf{M_L}$)*	4
2	06/03/2017	46.91 N	8.93 E	4	4.3 (4.6 $\mathbf{M_L}$)*	7
3	08/09/2005	46.04 N	6.89 E	4	4.4	15
4	05/12/2004	48.08 N	8.04 E	9	4.5	5
5	24/11/2004	45.69 N	10.52 E	5	5.0	5
6	23/02/2004	47.28 N	6.27 E	15	4.5	10
7	13/11/2002	45.59 N	10.15 E	10	4.2	3
8	17/07/2001	46.83 N	11.10 E	8	4.7	1
9	06/04/2000	46.53 N	10.36 E	5	4.0	4
10	31/12/1999	46.55 N	10.34 E	5	4.1	1
11	29/12/1999	46.55 N	10.30 E	5	4.9	5
12	31/03/1996	45.94 N	7.46 E	4	4.2	1

(The conversion relationship $\mathbf{M_W} = \mathbf{M_L} - 0.3$ is adopted for $\mathbf{M_L}$ above 4.0 [Goertz-Allmann *et al*., 2011])

All the recordings were taken from rock sites. Only recordings marked with moment magnitude larger than 4.0 (two of them were recorded in local moment and have been converted into moment magnitude) and rupture distance in the range: 1 km - 200 km have been selected. The epicentres of study events in Switzerland are shown in Fig. 16, and the magnitude-distance distribution of the selected ground motions is shown in Fig. 17.

The upper-crustal modification effect can be significant for modifying the spectral amplitude. To construct the shear-wave velocity profile with a reasonable degree of accuracy, the geology-based approach is adopted in this study [Chandler *et al*., 2005] (the updated model can be obtained by requests). The approach adopted by **CAM** can make best use of the geological information representing the study region. The modelling parameters of shear-wave velocity profile are listed in Table 5.

The detailed **Vs** profile model is expressed from Eqs. (16) to (19).

$$V_{S0.03}*(Z/0.03)^{0.3297} \qquad 0 < Z \leq Z_S \tag{16}$$

$$V_{SZc}*(Z/Z_C)^{n} \qquad Z_S < Z \leq Z_C \tag{17}$$

$$V_{S2}*(Z/2)^{0.0899} \qquad Z_C < Z \leq 2 \tag{18}$$

$$V_{S8}*(Z/8)^{0.0833} \qquad Z > 2 \tag{19}$$

$\mathbf{Z_S}$ and $\mathbf{Z_C}$ are defined as the thickness of upper sedimentary crustal layer and total sedimentary crustal layer, respectively; $V_{S0.03}$ and V_{S8} are defined as the V_S value at the depth of 0.03 km and 8 km respectively; *n* is the exponent in the non-linear functional form for constructing V_S profile.

The V_S data were collected from CRUST1.0 database [Laske *et al*., 2013] and previous publications [Campus and Fäh,1997; Fäh *et al*., 2003; Poggi *et al*., 2011] for Switzerland

region. The final V_S profile and the corresponding frequency-dependent amplification factor, together with the range obtained from V_{S30} = 0.76 km/s (NEHRP B/C site) and V_{S30} = 2.78 km/s (Generic Hard Rock site) using SRI (square-root-impedance) approach are shown in Fig. 18.

The upper-crustal attenuation effect (for κ_0 = 0.016 s) is based on recommendations by Edwards and Fäh [2003] for applications in Switzerland. It can be found that the shear-wave velocity profile obtained from this study is close to the study conducted by Poggi *et al.* [2011] (V_{S30} = 1.1 km/s) for Switzerland within the classification of NEHRP Site A. Comparison between the recorded data and estimates derived from **CAM** has been conducted for natural periods of 0.3 s and 1.0 s, for the considered earthquake events. Residuals of predictions were then calculated and compared (refer Figs. 19 and 20 respectively). In **CAM** the values of seismological parameters adopted for Switzerland conditions are listed in Table 6.

Table 5. Parameters for modelling shear-wave velocity profile for Switzerland.

Parameter	Value
Z_S (km)	0.01
Z_C (km)	0.62
$V_{S0.03}$ (km/s)	1.42
V_{S8} (km/s)	3.55
n	0.23

(More detailed information about Vs profile modelling can be obtained upon request to the authors)

Table 6. Parameters values in **CAM** for use in Switzerland.

Parameter	Value
Stress drop, $\Delta\boldsymbol{\sigma}$ (bar)	63 [Edwards and Fäh, 2013]
Geometric spreading factor, **G**	$0 \leq \mathbf{R} \leq 70, \quad \mathbf{R}^{-1.11}$ $70 < \mathbf{R} \leq \mathbf{120}, \quad \mathbf{R}^{-0.41}$ $120 < \mathbf{R}, \quad \mathbf{R}^{-1.38}$ $\mathbf{R} = \sqrt{\mathbf{R}_{rup}^2 + \mathbf{h}_{FF}^2})$ [Edwards *et al*., 2011]
Finite-fault factor, $\mathbf{h}_{FF}$	$10^{-0.405+0.235\mathbf{M}}$ [Yenier and Atkinson, 2014]
Anelastic attenuation factor, Q_0	1200 [Edwards *et al*., 2011]
NEHRP crust class, V_{S30} (km/s)	1.1
Upper-crustal attenuation, κ_0 (s)	0.016 [Edwards *et al*., 2011]
Middle-crustal modification factor, $\boldsymbol{\gamma_{mc}}$	1.086
Calibration factor (**C**)	0.2

Results presented in Fig. 19 show that **CAM** can predict RSA values at different natural periods for use in Switzerland with reasonable accuracy. The positive residuals at the distance between 40 and 100 km at T_n = 1.0 s is believed to be resulted from the paucity of data or some biases in the attenuation model adopted in **CAM**.

Conclusion

The Component Attenuation Model (**CAM**) belongs to a class of generic GMPEs which have parameters characterising the effects of stress behaviour at the source, geometrical spreading, anelastic attenuation and crustal modifications in addition to the usual magnitude-distance combination and site classification. The incorporation of the shear-wave velocity profile of the earth crust down to depth of 10 km and the associated wave amplification into **CAM** distinguishes itself from other generic models that have been published. **CAM** has been verified as a tool which is able to transform a diversity of seismological models into the respective GMPEs. Consistencies in predictions from **CAM** and from other generic GMPEs (that are denoted as **YA15** and **HA18**) have also been demonstrated. All these models consistently show systematic and significant differences in the response spectral behaviour between western and eastern North America. The accuracy of predictions by **CAM** has also been evaluated through comparison with 61 field records from 12 earthquake events that have occurred in Switzerland.

Data and Resources

All the electronic version of the data and GMSS platform can be made available upon requests. The recording data used in this study are obtained from SSS (Swiss Seismological Service) Strong Motion Portal (http://strongmotionportal.seismo.ethz.ch/home/, which was last accessed by the authors in January 2019).

Acknowledgements

The support of the Commonwealth of Australia through the Cooperative Research Centre program is sincerely acknowledged. The financial support from China Scholarship Council (CSC) for the first author is sincerely acknowledged. The suggestion of using Swiss earthquake recording data is from Earthquake Engineering and Structural Dynamics (EESD) Laboratory in ÉCOLE POLYTECHNIQUE FÉDÉRALE DE LAUSANNE (EPFL), which is sincerely acknowledged.

References

Akkar, S. and Bommer, J.J. [2010] "Empirical equations for the prediction of PGA , PGV, and Spectral Accelerations in Europe, the Mediterranean Region, and the Middle East," *Seismol. Research Letters* **81**(2), 195-206.

Akkar, S., Sandikkaya, M.A. and Bommer, J.J. [2014] "Empirical ground-motion models for point- and extended-source crustal earthquake scenarios in Europe and the Middle East," *Bull. Earthquake Eng.* **12**(1), 359-387.

Allen, T. I. [2012] *Stochastic ground-motion prediction equations for southeastern Australian earthquakes using updated source and attenuation parameters*. Geoscience Australia. Canberra.

Ambraseys, N. N., Douglas, J., Sarma, S. K. and Smit, P.M. [2005] "Equations for the estimation of strong ground motions from shallow crustal earthquakes using data from Europe and Middle East: Horizontal Peak Ground Acceleration and Spectral Acceleration," *Bull. Earth. Eng.* **3**, 1-53.

Atkinson, G. M. [1993] "Earthquake source spectra in Eastern North America," *Bull. Seismol. Soc. Am.* **88**(6), 1778-1798.

Atkinson, G. M. [2004] "Empirical attenuation of ground-motion spectral amplitudes in Southeastern Canada and the Northeastern United States," *Bull. Seism. Soc. Am.* **94**, 1079-1095.

Atkinson, G. M. [2008] "Ground-motion prediction equations for Eastern North America from a referenced empirical approach: Implications for epistemic uncertainty," *Bull. Seismol. Soc. Am.* **98**(3), 1304-1318.

Atkinson, G. M. and Boore, D. M. [1995] "Ground-motion relations for Eastern North America," *Bull. Seismol. Soc. Am.* **85**(1), 17-30.

Atkinson, G. M. and Boore, D. M. [1998] "Evaluation of models for earthquake source spectra in Eastern North America," *Bull. Seismol. Soc. Am.* **88**(4), 917-934.

Atkinson, G. M. and Boore, D. M. [2006] "Earthquake ground-motion prediction equations for Eastern North America," *Bull. Seismol. Soc. Am.* **96**(6), 2181-2205.

Atkinson, G.M. and Boore, D.M. [2011] "Modifications to existing ground-motion prediction equations in light of new data," *Bull. Seismol. Soc. Am.* **101**(3), 1121-1135.

Atkinson, G.M. and Boore, D.M. [2014] "The attenuation of Fourier amplitudes for rock sites in Eastern North America," *Bull. Seism. Soc. Am.* **104**, 513-528.

Atkinson, G.M. and Motazedian, D. [2013] "Ground-motion amplitudes for earthquakes in Puerto Rico," *Bull. Seismol. Soc. Am.* **103**(3), 1846-1859.

Atkinson, G.M. and Silva, W.J. [2000] “Stochastic modeling of California ground motions,” *Bull. Seismol. Soc. Am.* **90**(2), 255-274.

Bay, F., Fäh, D., Malagnini, L. and Giardini, D. [2003] “Spectral shear-wave ground-motion scaling in Switzerland,” *Bull. Seismol. Soc. Am.* **93**(1), 414-429.

Boatwright, J. and Seekins, L. [2011] “Regional spectral analysis of three moderate earthquakes in Northeastern North America,” *Bull. Seism. Soc. Am.* **101**, 1769-1782.

Boore, D. M. [2003] “Simulation of ground motion using the stochastic method,” *Pure Appl. Geophys.* **160**, 635-676.

Boore, D.M. [2015] *Point-Source Stochastic-Method Simulations of Ground Motions for the PEER NGA-East Project. PEER Rept. No. 2015/04, Chapter 2*. California, Pacific Earthquake Engineering Research Center, University of California, Berkeley.

Boore, D.M. [2016] “Short Note: Determining generic velocity and density models for crustal amplification calculations, with and update of Boore and Joyner (1997) generic site amplification for Vs(z) = 760 m/s,” *Bull. Seismol. Soc. Am.* **106**(1), 316-320.

Boore, D.M., Alessandro, C.D. and Abrahamson, N.A. [2014] “A generalization of the double-corner-frequency source spectral model and its use in the SCEC BBP validation exercise,” *Bull. Seismol. Soc. Am.* **104**(5), 2387-2398.

Boore, D.M. and Atkinson, G.M. [1992] “Source spectra for the 1988 Saguenay, Quebec, earthquakes,” *Bull. Seismol. Soc. Am.* **82**(2), 683-719.

Boore, D.M., Campbell, K.W. and Atkinson, G.M. [2010] “Determination of stress parameters for eight well-recorded earthquakes in Eastern North America,” *Bull. Seism. Soc. Am***. 100**, 1632-1645.

Boore, D.M. and Joyner, W.B. [1997] “Site amplification for generic rock sites,” *Bull. Seismol. Soc. Am.* **87**(2), 327-341.

Boore, D.M., Stewart, J.P., Seyhan, E. and Atkinson, G.M. [2014] “NGA-West2 equations for predicting PGA, PGV, and 5% damped PSA for shallow crustal earthquakes,” *Earthquake Spectra* **30**(3), 1057-1085.

Brocher, T.M. [2005] “Empirical relations between elastic wavespeeds and density in the earth's crust,” *Bull. Seismol. Soc. Am.* **95**(6), 2081-2092.

Campbell, K. W. [2003] “Prediction of strong ground motion using the hybrid empirical method and its use in the development of ground-motion (attenuation) relations in Eastern North America,” *Bull. Seismol. Soc. Am.* **93**(3), 1012-1033.

Campus, P. and Fäh, D. [1997] “Seismic monitoring of explosions: A method to extract information on the isotropic component of the seismic source,” *J. Seismol.* **1**, 205-218.

Chandler, A.M., Lam, N.T.K. and Tsang, H.H. [2005] "Shear wave velocity modelling in crustal rock for seismic hazard analysis," *Soil Dynamics and Earthquake Engineering* **25**(2), 167-185.

Chandler, A.M., Lam, N.T.K. and Tsang, H.H. [2006a] "Regional and local factors in attenuation modelling: Hong Kong case study," *Journal of Asian Earth Sciences* **27**(6), 892-906.

Chandler, A.M., Lam, N.T.K. and Tsang, H.H. [2006b] "Near-surface attenuation modelling based on rock shear-wave velocity profile," *Soil Dynamics and Earthquake Engineering* **26**, 1004-1014.

Drouet, S., Cotton, F. and Guéguen, P. [2010] "V_{S30}, κ, regional attenuation and **Mw** from accelerograms: Application to magnitude 3–5 French earthquakes," *Geophys. J. Inter.* **182**(2), 880-898.

Edwards, B., Fäh, D. and Giardini, D. [2011] "Attenuation of seismic shear wave energy in Switzerland," *Geophys. J.Inter* **185**(2), 967-984.

Fäh, D., Kind, F. and Giardini, D. [2003] "Inversion of local S-wave velocity structures from average H/V Ratios, and their use for the estimation of site-effects," *J. Seismol.* **7**, 449-467.

Goertz-Allmann, B. P., Edwards, B., Bethmann, F., Deichmann, N., Clinton, J., Fäh, D. and Giardini, D. [2011] "Short Note: A new empirical magnitude scaling relation for Switzerland," *Bull. Seismol. Soc. Am.* **101**(6), 3088-3095.

Hassani, B. and Atkinson, G.M. [2015] "Referenced empirical ground-motion model for Eastern North America," *Seismological Research Letters* **86**(2A), 477-491.

Hassani, B. and Atkinson, G. M. [2018] "Adjustable generic ground-motion prediction equation based on equvilent point-source simulations: Accounting for kappa effects," *Bull. Seismol. Soc. Am.* **108**(2), 913-928.

Lam, N.T.K., Wilson, J.L. and Hutchinson, G. [2000a] "Generation of synthetic earthquake accelerograms using seismological modelling: A review," *Journal of Earthquake Engineering* **4**(3), 321-354.

Lam, N. T. K., Wilson, J.L., Chandler, A.M. and Hutchinson, G. [2000b] "Response spectral relationships for rock sites derived from the component attenuation model," *Journal of Earthquake Engineering & Structural Dynamics* **29**, 1457-1489.

Laske, G., Ma, Z., Masters, G. and Pasyanos, M. [2013] *CRUST 1.0: A New Global Crustal Model at 1×1 Degrees*, https://igppweb.ucsd.edu/~gabi/crust1.html.

Mak, S., Chan, L.S., Chandler, A.M. and Koo, R. [2004] "Coda Q estimates in the Hong Kong Region," *Journal of Asian Earth Sciences* **24**, 127-136.

Morasca, P., Malagnini, L., Akinci, A., Spallarossa, D. and Herrmann, R.B. [2006] "Ground-motion scaling in the Western Alps," *J. Seismol.* **10**, 315-333.

PEER. [2015] *NGA-East: Median Ground-Motion Models for the Central and Eastern North America Region*, University of California, Berkeley.

Pezeshk, S., Zandieh, A., Campbell, K. W., Tavakoli, B. [2015] *Ground motion prediction equations for CENA using the hybrid empirical method in conjunction with NGA-West2 empirical ground motion models, in NGA-East: Median Ground Motion Models for the Central and Eastern North America Region. PEER Rept. No. 2015/04, Chapter 5*. California, Pacific Earthquake Engineering Research Center, University of California, Berkeley.

Poggi, V., Edwards, B. and Fäh, D. [2011] "Derivation of a refenrence shear-wave velocity model from empirical site amplification," *Bull. Seismol. Soc. Am.* **101**(1), 258-274.

Rietbrock, A., Strasser, F. and Edwards, B. [2013] "A stochastic earthquake ground-motion prediction model for the United Kingdom," *Bull. Seismol. Soc. Am.* **103**(1), 57-77.

Seyhan, E. and Stewart, J. P. [2014] "Semi-empirical nonlinear site amplification from NGAWest2 data and simulations," *Earthq. Spectra* **30**, 1241-1256.

Silva, W., Gregor, N.N. and Darragh, R.B. [2002] "Development of regional hard rock attenuation relations for Central and Eastern North America," *Report to Pacific Engineering and Analysis.*

Silva, W.J., Gregor, N.N. and Darragh, R.B. [1999] *Reassessment of Site Coefficients and Near-Fault Factors for Building Code Provisions. Final Technical Report.* N. E. R. Program. El Cerrito, CA.

Singh, S. K., Garcı´a, D., Pacheco, J. F., Valenzuela, R., Bansal, B.K., Dattatrayam, R.S. [2004] "Q of the Indian Shield," *Bull. Seismol. Soc. Am.* **94(4)**, 1564-1570.

Tang, Y., Lam, N.T.K., Tsang, H.H. and Lumantarna, E. [2017] "A generic approach to ground motion predictions," *Proc. of Australian Earthquake Engineering Society 2017 Conference*. Canberra, ACT.

Tsang, H.H., Sheikh, N. and Lam, N.T.K. [2010] "Regional differences in attenuation modelling for Eastern China," *Journal of Asian Earth Sciences* **39(5)**, 451- 459.

Van, H. C., Drouet, S. and Cotton, F. [2011] "Analysis of the origins of κ (kappa) to compute hard rock to rock adjustment factors for GMPEs," *Bull. Seismol. Soc. Am.* **101**(6), 2926-2941.

Yenier, E. and Atkinson, G. M. [2014] "Equivalent point-source modelling of moderate-to-large magnitude earthquakes and associated ground-motion saturation effects," *Bull. Seismol. Soc. Am.* **104**(3), 1458-1478.

Yenier, E. and Atkinson, G. M. [2015a] "An equivalent point-source model for stochastic simulation of earthquake ground motions in California," *Bull. Seismol. Soc. Am.* **105**(3), 1435-1455.

Yenier, E. and Atkinson, G.M. [2015b] “Regionally adjustable generic ground-motion prediction equation based on equivalent point-source simulations: application to Central and Eastern North America,” *Bull. Seismol. Soc. Am.* **105**(4), 1989-200

Table I. Summary of the selected NGA-East GMMs (PEER 2015, Yenier and Atkinson 2015b)

Geometric spreading functions	R	Q	Applicable range	Model and Reference
$R \le 70, G(R) = R^{-1}$; $70 \le R \le 130, G(R) = 70^{-1} * (\frac{R}{70})^{0}$; $R > 130, G(R) = 70^{-1} * 130^{0} * (\frac{R}{130})^{-0.5}$	$R = R_{hyp}$	$680f^{0.36}$	*4.0 ≤ M ≤ 7.25* *10 ≤ R ≤ 500* *0.5 ≤ f ≤ 20*	**AB95** [Atkinson and Boore, 1995]
$R \le 80, G(R) = R^{-(1.0296-0.0422(M-6.5))}$ $R > 80, G(R) = 80^{-(1.0296-0.0422(M-6.5))} * R^{-0.5*(1.0296-0.0422(M-6.5))}$	$R = R_{hyp}$	$351f^{0.84}$	*4.5 ≤ M ≤ 8.5* *1 ≤ R ≤ 400* *0.1 ≤ f ≤ 100*	**SGD02** [Silva *et al.*, 2002]
$R \le 70, G(R) = R^{-1.3}$ $70 \le R \le 140, G(R) = 70^{-1.3} * (\frac{R}{70})^{0.2}$; $R > 140, G(R) = 70^{-1} * 140^{0.2} * (\frac{R}{140})^{-0.5}$	$R = R_{hyp}$	$max(1000, 893f^{0.32})$	*4.4 ≤ M ≤ 6.8* *10 ≤ R ≤ 800* *0.05 ≤ f ≤ 20*	**A04** [Atkinson 2004]
$G(R) = R^{-1}$, *for all* ***R***	$R = (R_{hyp}{}^2 + h_{FF}{}^2)^{0.5}$, $h_{FF} = 10^{-0.405+0.235M}$	2850	*4.4 ≤ M ≤ 6.8* *10 ≤ R ≤ 800* *0.05 ≤ f ≤ 20*	**BCA10d** [Boore *et al.*, 2010]
$R \le 50, G(R) = R^{-1}$; $R > 50, G(R) = 50^{-1} * (\frac{R}{50})^{-0.5}$	$R = R_{hyp}$	$410f^{0.5}$	*4.4 ≤ M ≤ 5.0* *23 ≤ R ≤ 602* *0.2 ≤ f ≤ 20*	**BS11** [Boatwright and Seekings, 2011]
$R \le 50, G(R) = 10^{T_C C_{LF}} R^{-1.3}$; $R > 50, G(R) = 50^{-1.3} * (\frac{R}{50})^{-0.5} f \le 1, T_C = 1; 1 < f < 5, T_C = 1 - 1.429 \log(f)$; $f \ge 5, T_C = 0. R \le h, C_{LF} = 0.2 \cos((\pi/2)(R-h)/(1-h))$; $10 < R < 50, C_L = 0.2 \cos(((\pi/2)(R-h)/(1-h))$;	$R = (R_{hyp}{}^2 + h_{FF}{}^2)^{0.5}$, $h_{FF} = 10^{-0.405+0.235M}$ h = focal depth	$525f^{0.45}$	*3.5 ≤ M ≤ 6.0* *10 ≤ R ≤ 500* *0.2 ≤ f ≤ 20*	**AB14** [Atkinson, 2014]
$R \le 50, G(R) = R^{-1.3}$; $R > 50, G(R) = 50^{-1.3} * (\frac{R}{50})^{-0.5}$	$R = (R_{rup}{}^2 + h_{FF}{}^2)^{0.5}$ $h_{FF} = 10^{-0.405+0.235M}$	$\gamma_f R_{rup}$	*3.0 ≤ M ≤ 8.0* *1 ≤ R ≤ 600* *0.1 ≤ f ≤ 100*	**YA15** [Yenier and Atkinson, 2015b]

Appendix

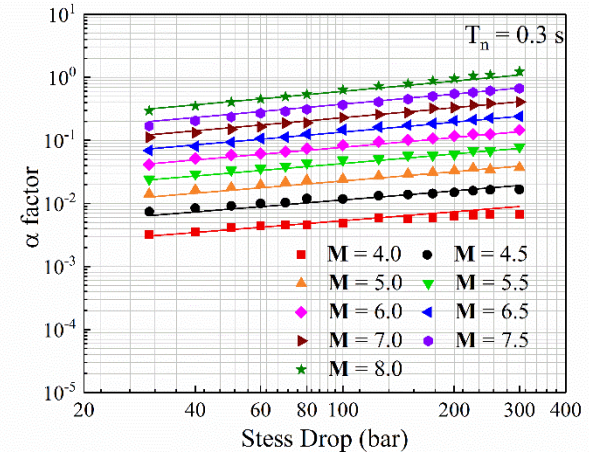

(a) T_n = 0.3 s

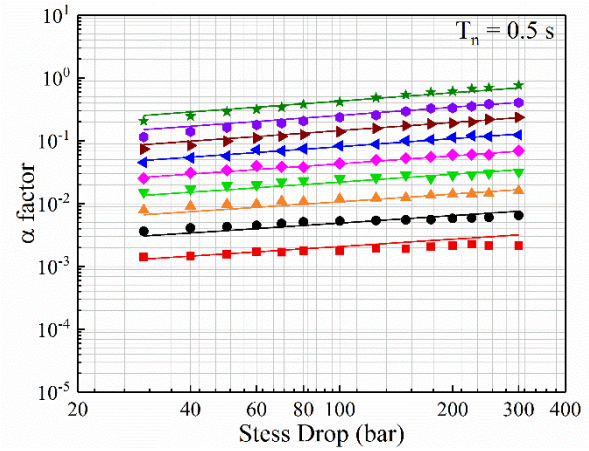

(b) T_n = 0.5 s

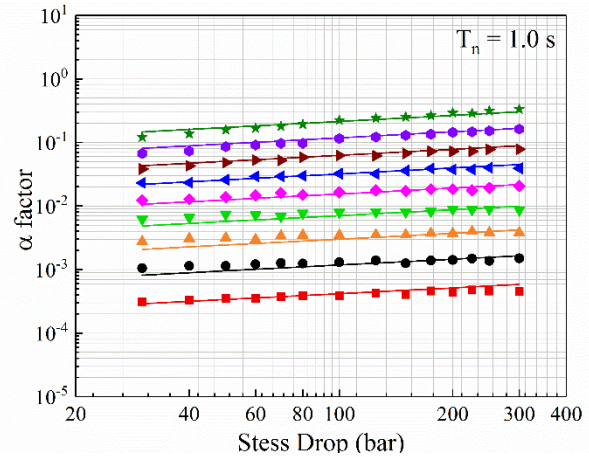

(c) T_n = 1.0 s

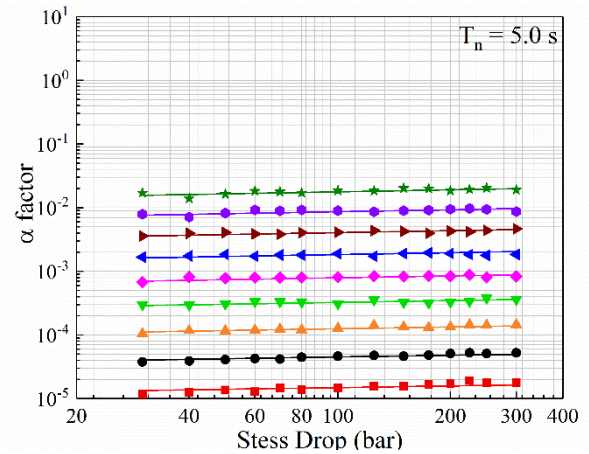

(d) T_n = 5.0 s

Figure 1. Simulated values of **α** factor normalized at **M** = 6 (symbols) shown alongside predictions by **CAM** (curves) for varying moment magnitude and stress drop, at **R** = 30 km.

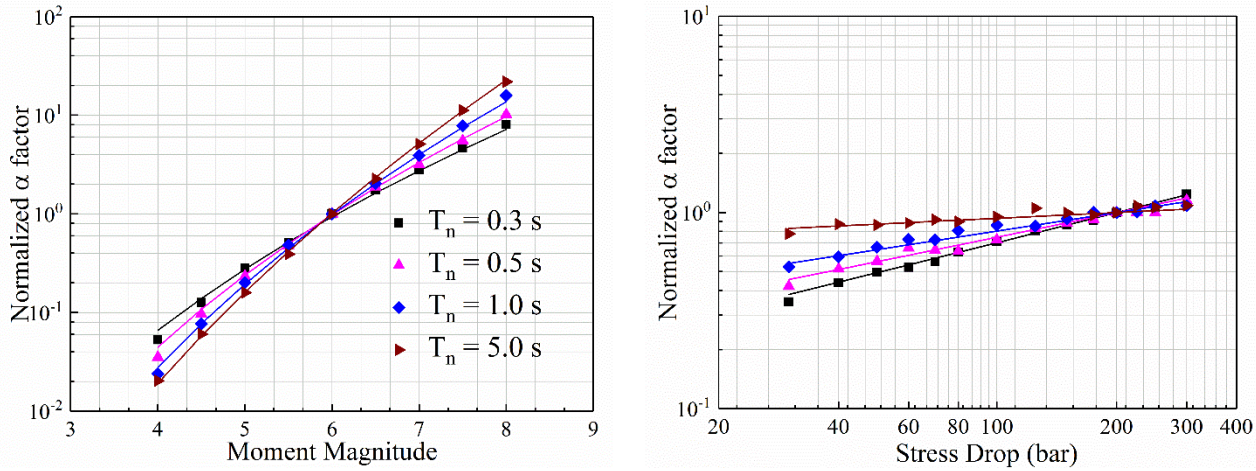

(a) **M** = 6 (b) Δ***σ***=200 bar

Figure 2. Simulated values of α factor normalized at **M** = 6 (a) and Δ***σ***=200 bar (b) (symbols) shown alongside predictions by **CAM** (curves) as a function of moment magnitude (a) and stress drop (b), at **R** = 30 km.

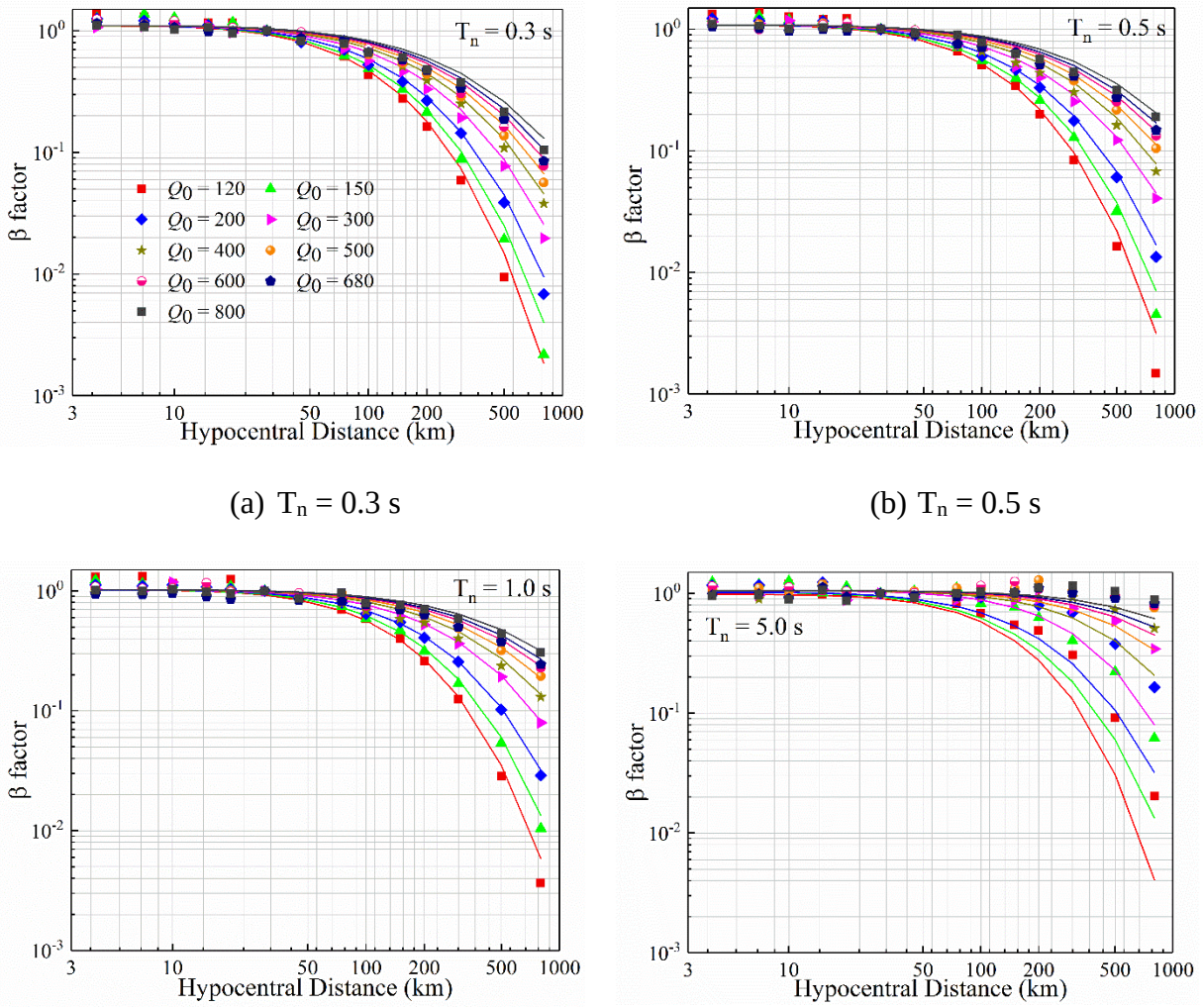

(a) T_n = 0.3 s

(b) T_n = 0.5 s

(c) T_n = 1.0 s

(d) T_n = 5.0 s

Figure 3. Stochastically simulated values of **β** (symbols) shown for comparison with predictions by equation (11) of **CAM** (curves) for **M** = 6 and varying values of Q_0.

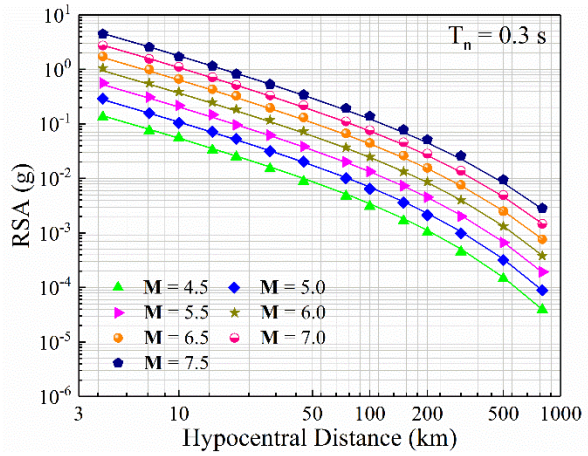

(a) T_n = 0.3 s

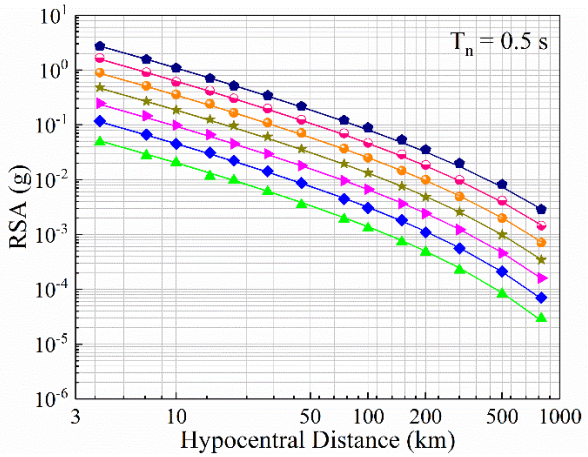

(b) T_n = 0.5 s

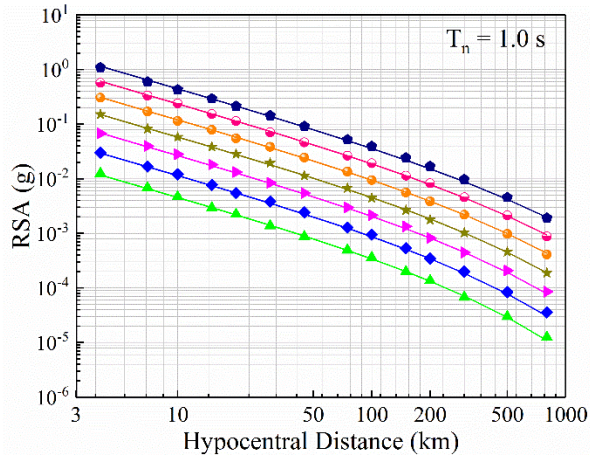

(c) T_n = 1.0 s

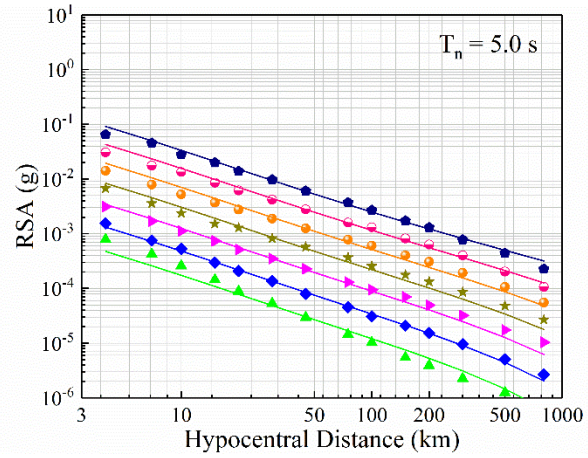

(d) T_n = 5.0 s

Figure 4. Simulated values of RSA normalised at **M** = 6 (symbols) for varying moment magnitudes and distances shown alongside predictions by **CAM** (curves) for Q_0 = 680, **G** = 1/**R**.

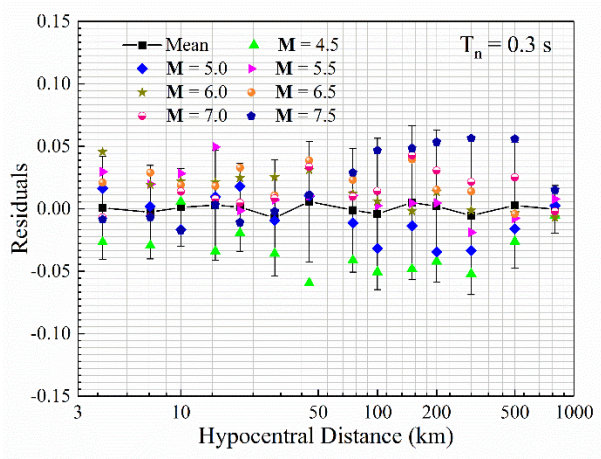

(a) T_n = 0.3 s

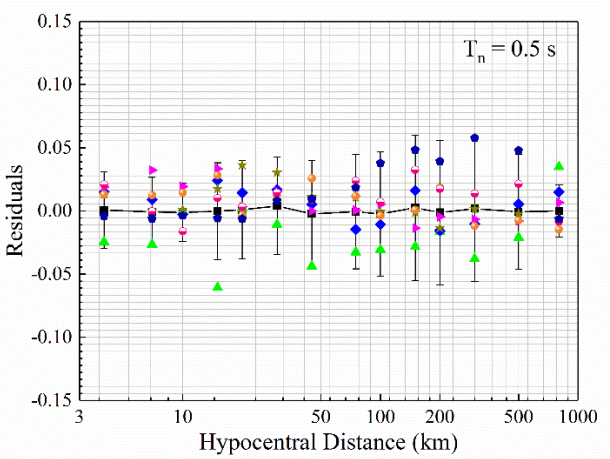

(b) T_n = 0.5 s

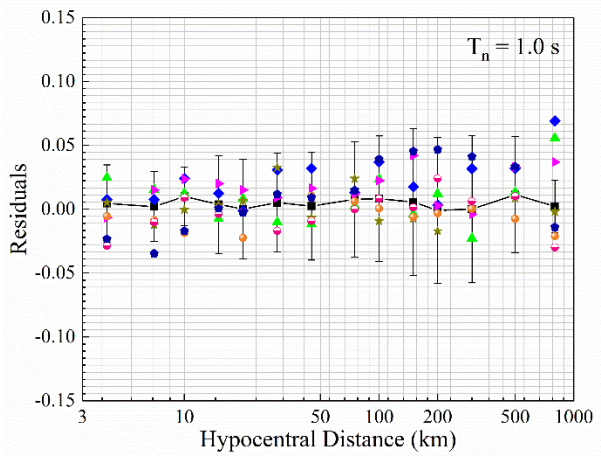

(c) T_n = 1.0 s

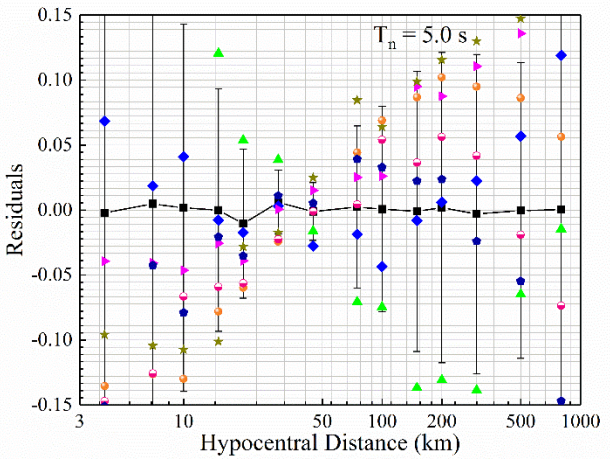

(d) T_n = 5.0 s

Figure 5. Results of residual analysis (based on the dataset presented in Fig. 4). Black squares denote *mean of residuals* whereas error bars denote *standard error about the mean*.

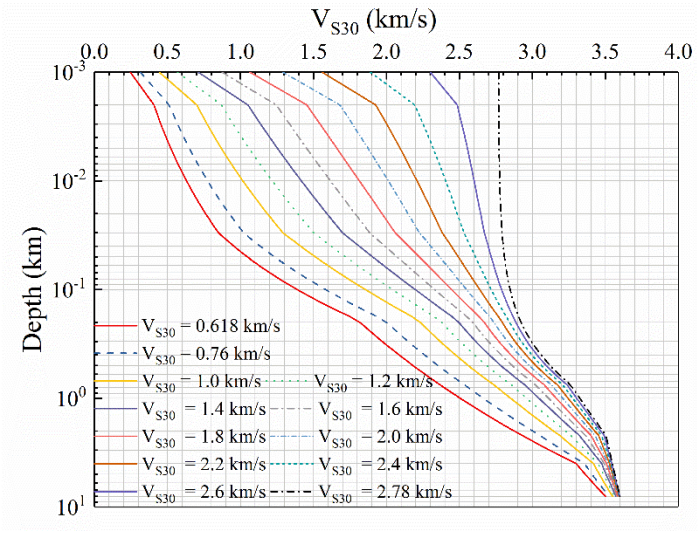

Figure 6. Shear wave velocity profiles considered in this study.

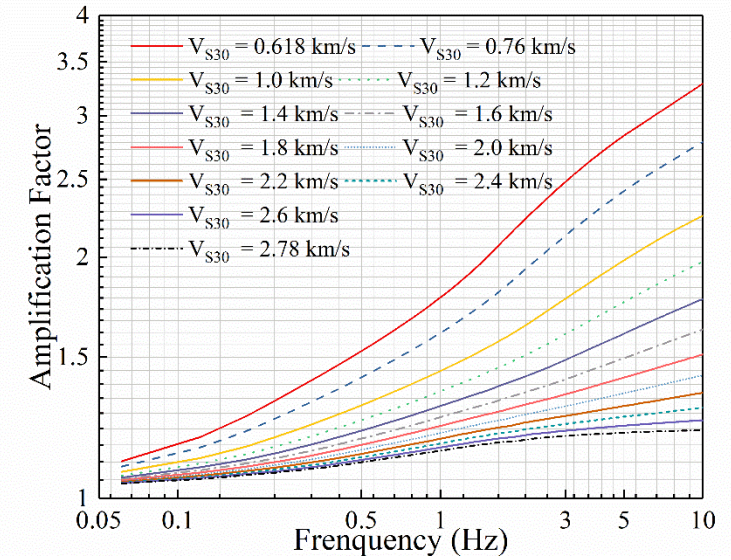

Figure 7. Frequency dependent amplification factor.

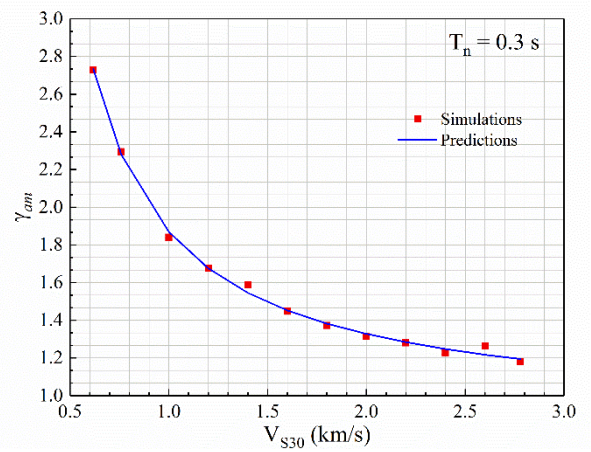

(a) T_n = 0.3 s

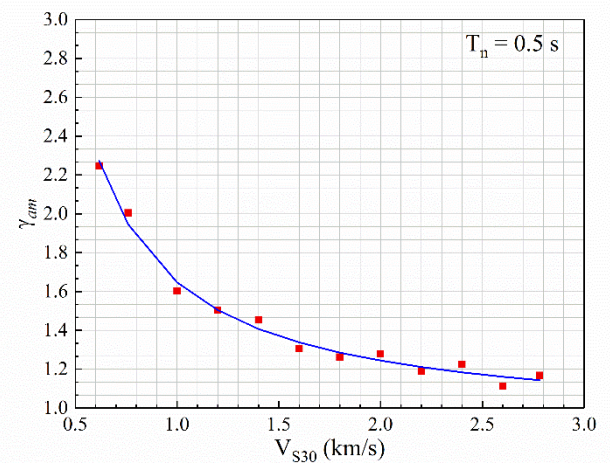

(b) T_n = 0.5 s

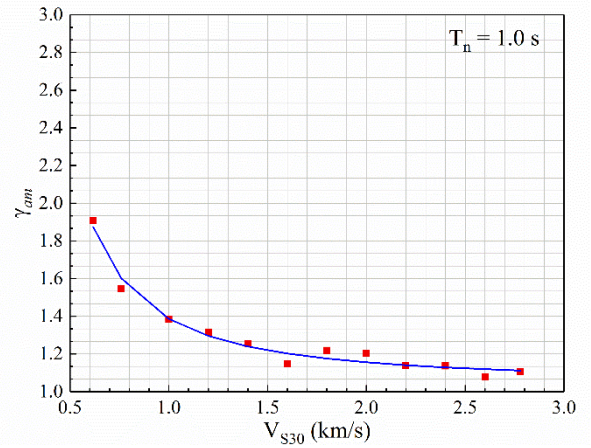

(c) T_n = 1.0 s

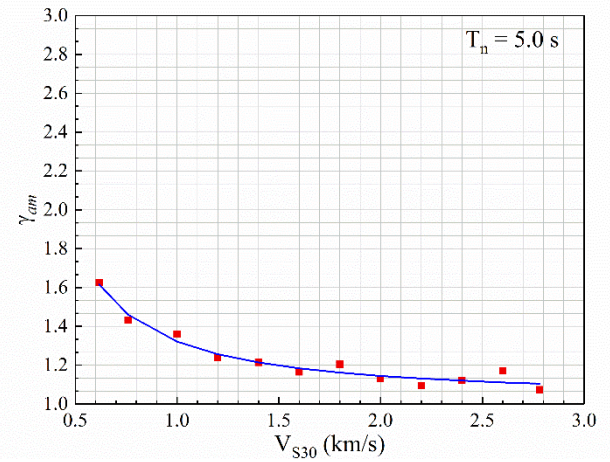

(d) T_n = 5.0 s

Figure 8. Trends of upper-crustal amplification factor ($\boldsymbol{\gamma_{am}}$).

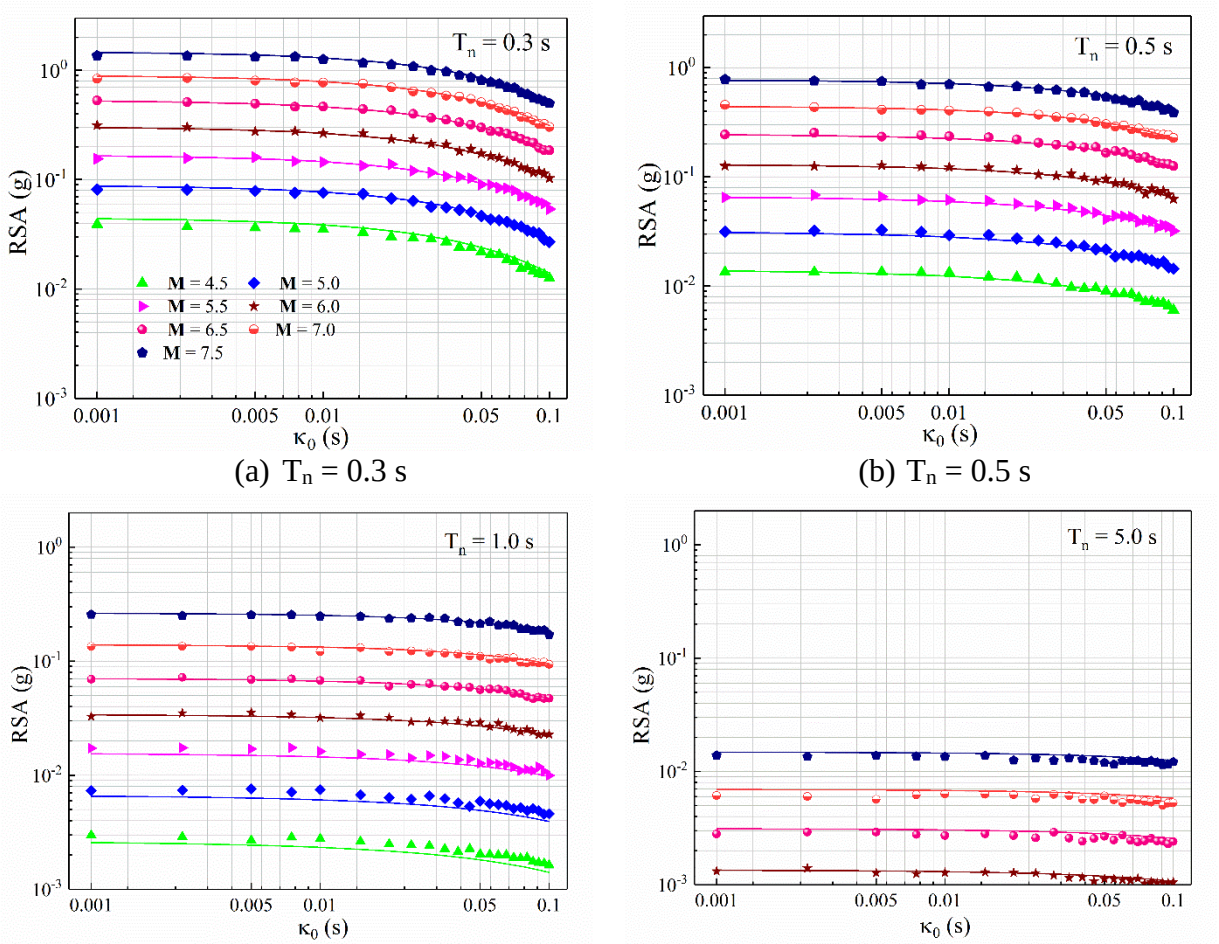

(a) T_n = 0.3 s (b) T_n = 0.5 s

(c) T_n = 1.0 s (d) T_n = 5.0 s

Figure 9. Simulated values of RSA (symbols) shown alongside predictions by **CAM** (curves) for κ_0 = 0.001s - 0.1s, $\Delta\sigma$=200 bar, **R**=30 km, on generic rock sites.

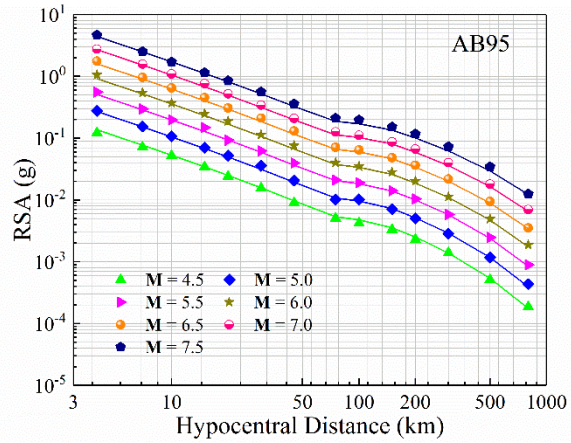

(a) **AB95**

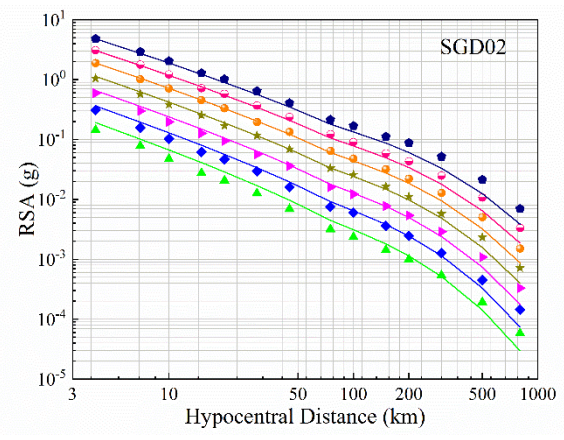

(b) **SGD02**

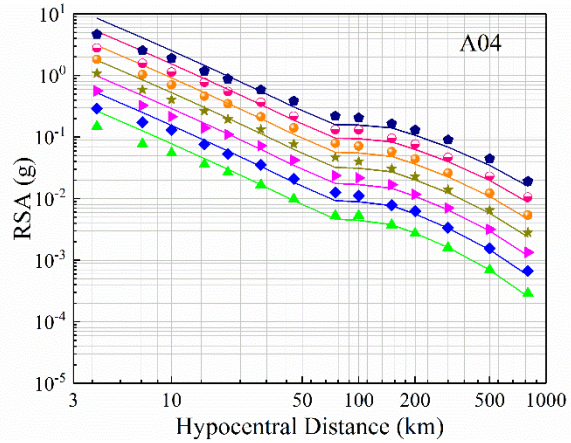

(c) **A04**

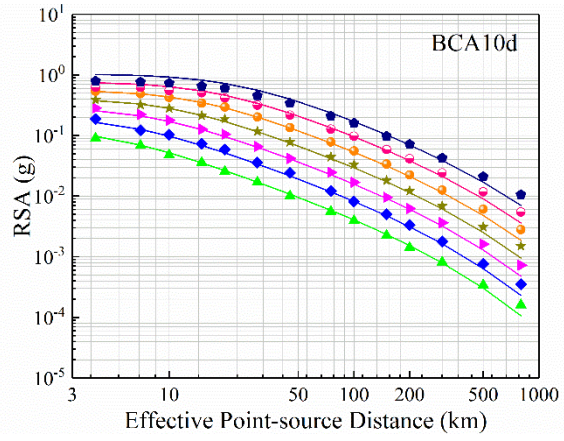

(d) **BCA10d**

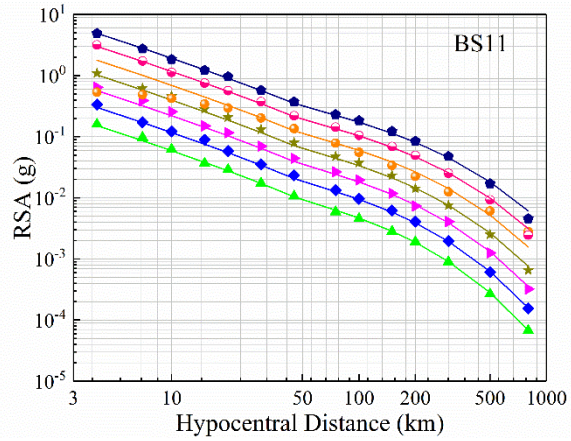

(e) **BS11**

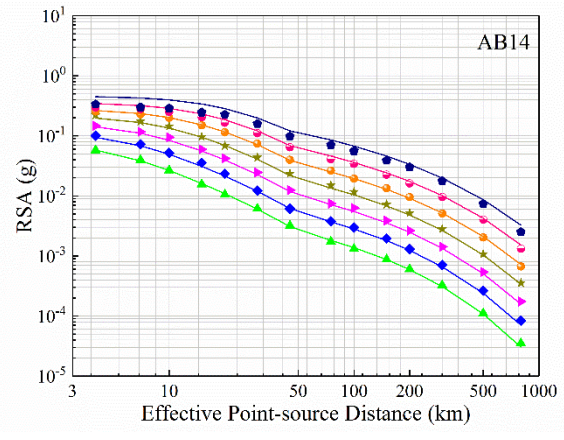

(f) **AB14**

Figure 10. Comparison between predictions by **CAM** (curves) and simulations of **six selected seismological models** (symbols). For the length limit of the paper, the results shown above are for RSA values at T_n = 0.3 s without crustal factor.

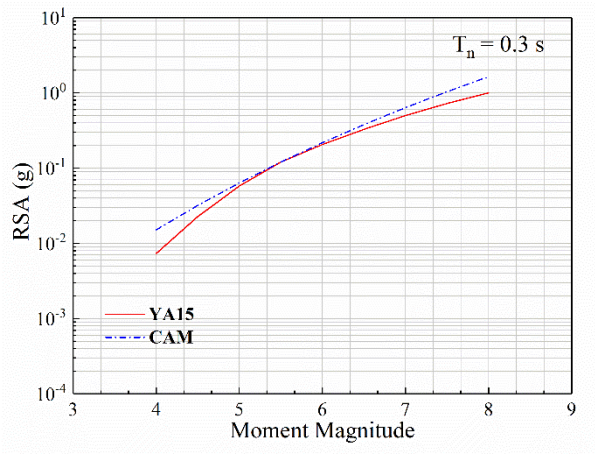

(a) T_n = 0.3 s

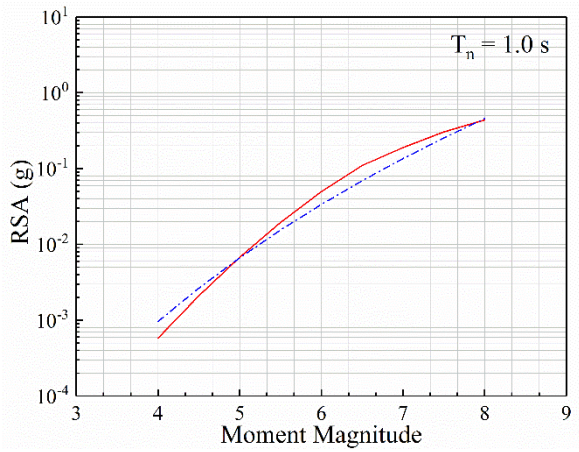

(b) T_n = 1.0 s

Figure 11. Comparison of predictions by **YA15** and **CAM** for varying magnitudes ($\Delta\sigma$ = 200 bars).

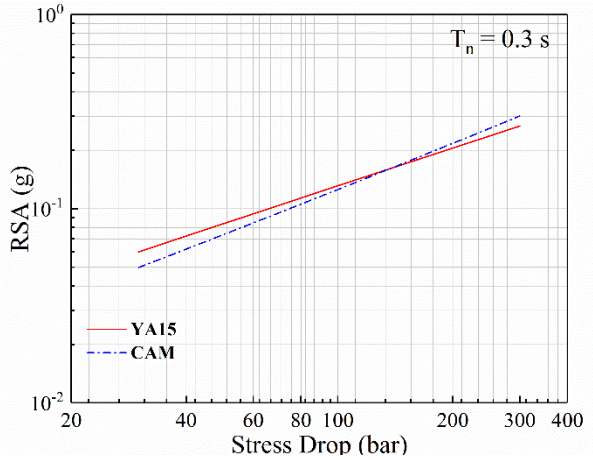

(a) T_n = 0.3 s

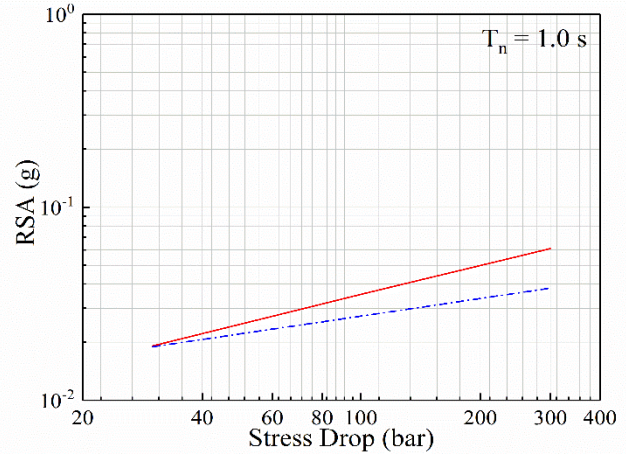

(b) T_n = 1.0 s

Figure 12. Comparison of predictions by YA15 and CAM for varying stress parameter values (M = 6 and R = 30 km).

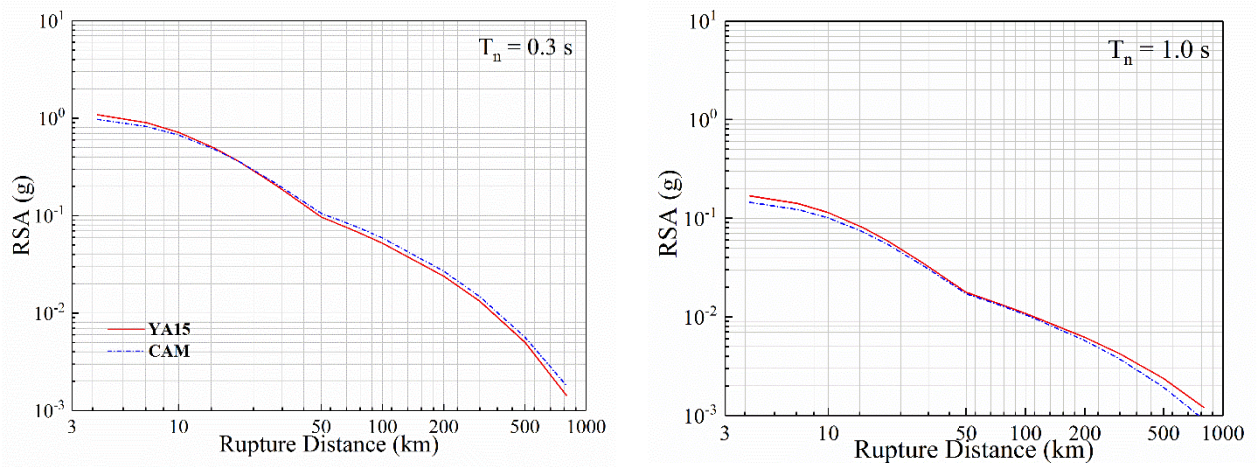

(a) T_n = 0.3 s (b) T_n = 1.0 s

Figure 13. Comparison of predictions by **YA15** and **CAM** for varying distance (**M** = 6 and **Δσ** = 200 bars).

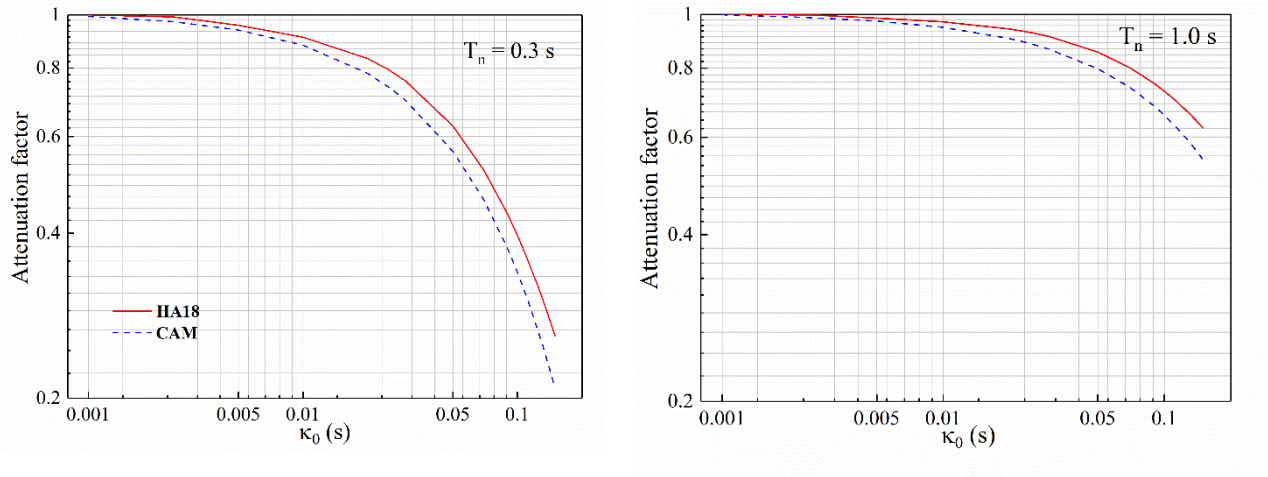

(a) T_n = 0.3 s (b) T_n = 1.0 s

Figure 14. Comparison of predictions by **HA18** and **CAM** for varying κ_0 values (**M** = 6, **R** = 30 km and **Δσ** = 200 bars).

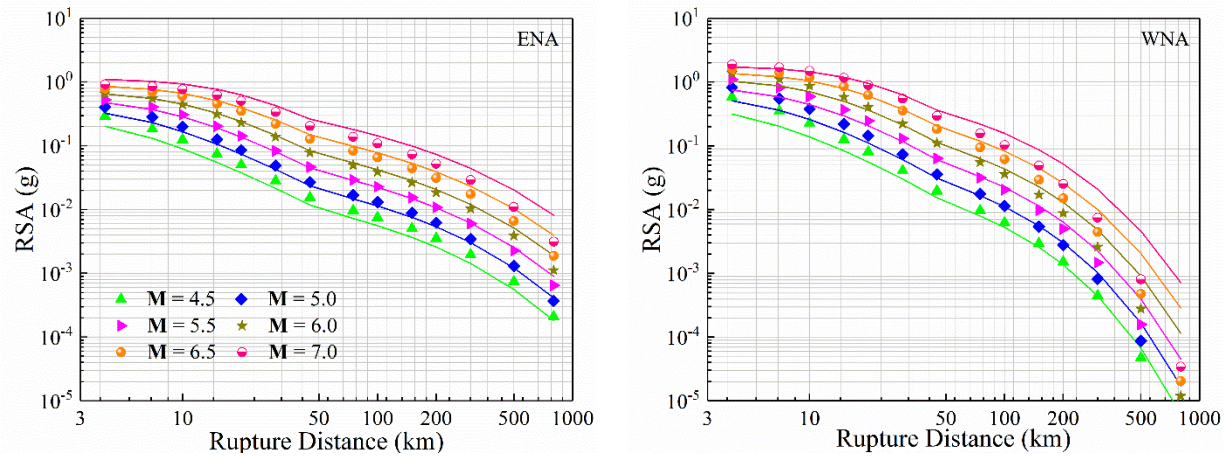

(a) ENA (b) WNA

Figure 15. Comparison between predictions by **CAM** (curves) and simulations of **YA15** model (symbols) for both ENA (Q_0 = 680, NEHRP A site with unit upper-crustal modification factor) and WNA (Q_0 = 150, NEHRP B/C site with V_{S30} = 0.76 km/s and κ_0 = 0.025 s) conditions.

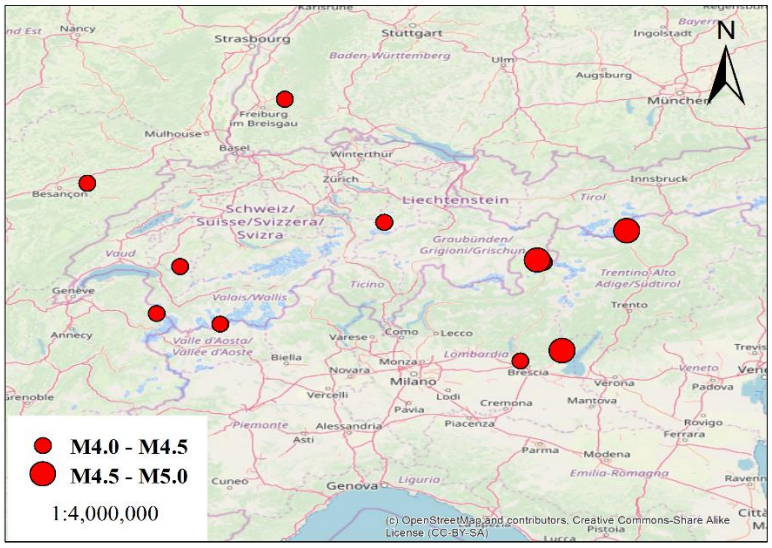

Figure 16. Epicentres of study events in Switzerland.

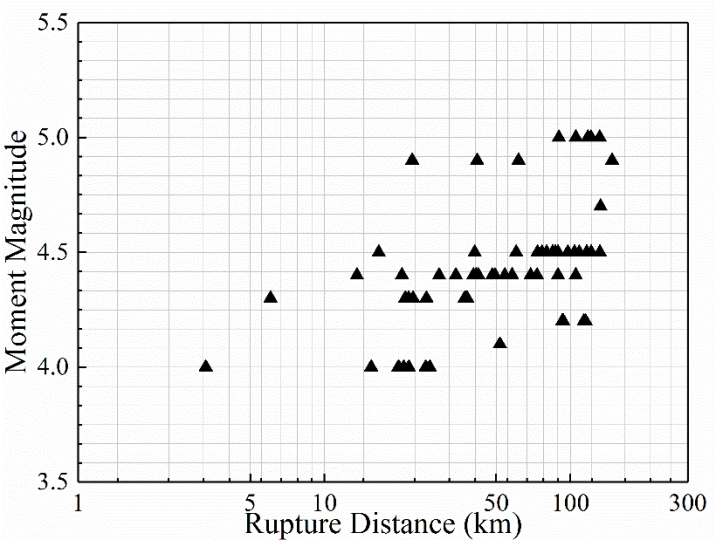

Figure 17. Magnitude-distance distribution of the selected ground motions in Switzerland.

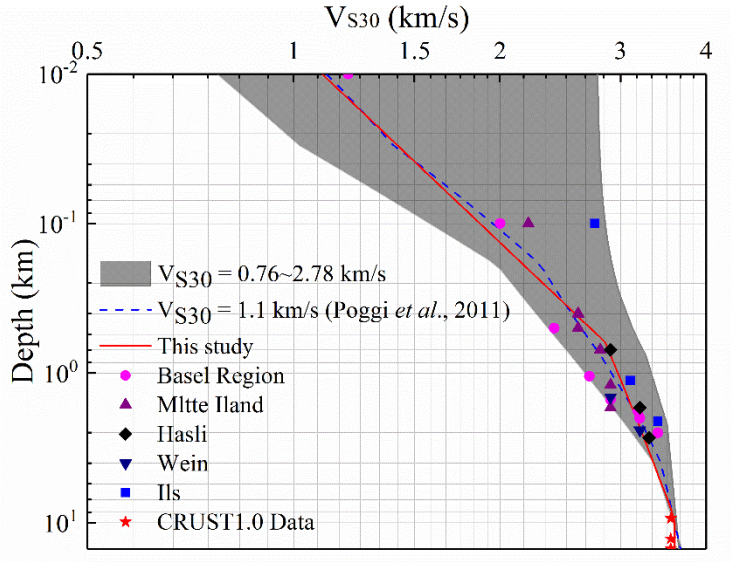

(a) Shear-wave velocity profile for Switzerland; shaded area is the range: V_{S30} = 0.76km/s (Generic Rock Site) - V_{S30} = 2.78 km/s (Generic Hard Rock Site). V_{S30} = 1.1 km/s is adopted.

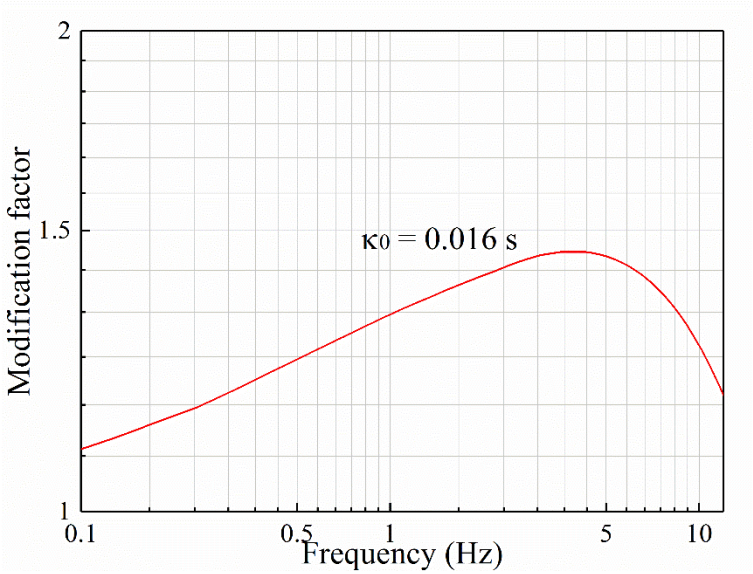

(b) Crustal modification factor taking κ_0 = 0.016 s.

Figure 18. Crustal profiles and corresponding amplification factors for studied regions.

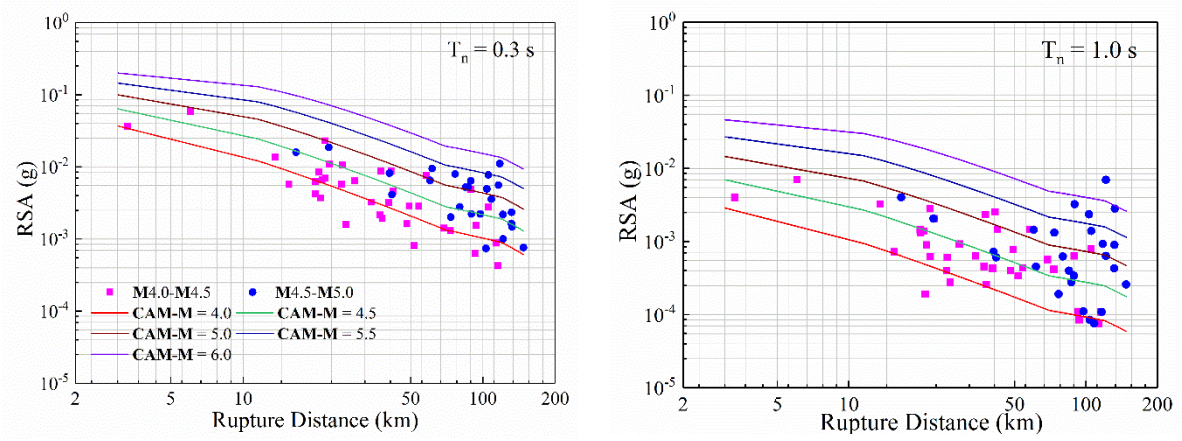

(a) T_n = 0.3 s

(b) T_n = 1.0 s

Figure 19. Comparison with recorded data for RSA in Switzerland on rock site.

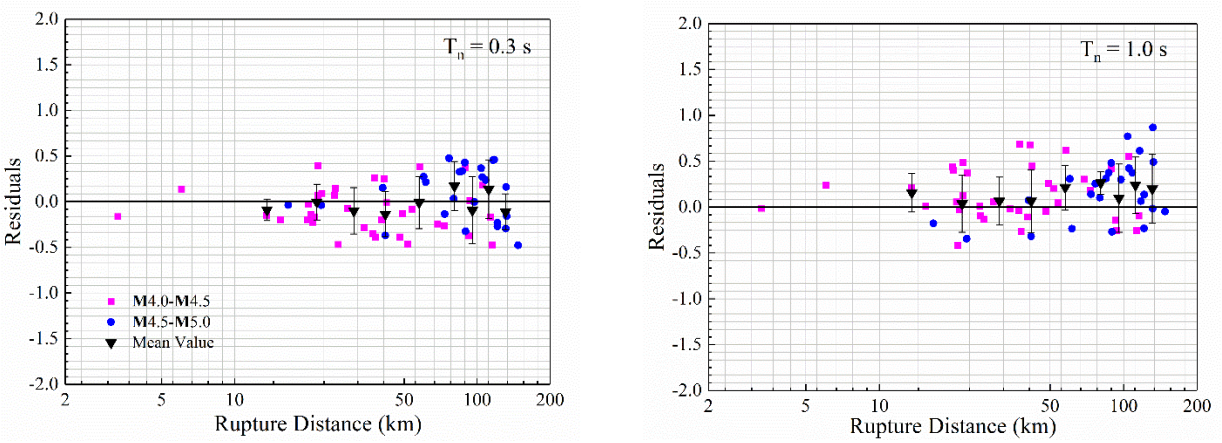

(a) T_n = 0.3 s (b) T_n = 1.0 s

Figure 20. Residuals of recorded data and predicted RSA obtained by **CAM** (residual = $\log_{10}$ (recorded RSA/ predicted RSA)). Mean and standard deviation values were calculated at rupture distances of 13.6, 21.8, 31.0, 41.8, 57.7, 80.5, 95.6, 111.7 and 131.0 km.